Final Report
on
Hazards Monitoring
At NASA Merritt Island Launch Area

VOLUME IV

GPO PRICE $ _____

CFSTI PRICE(S) $ _____

Hard copy (HC) 3.00

Microfiche (MF) 1.30

ff 653 July 65

FACILITY FORM 602

N67 14917 (ACCESSION NUMBER)

80 (PAGES)

CR-80957 (NASA CR OR TMX OR AD NUMBER)

1 (THRU)

(CODE)

14 (CATEGORY)

MELPAR INC

A SUBSIDIARY OF WESTINGHOUSE AIR BRAKE COMPANY

3000 ARLINGTON BOULEVARD, FALLS CHURCH, VIRGINIA

Final Report
on
Hazards Monitoring
At NASA Merritt Island Launch Area

VOLUME IV

Task D -- Measurements of Incident and Reflected UV and IR Electromagnetic Background at Saturn Complex

Contract No. NAS10-2009

National Aeronautics and Space Administration
John F. Kennedy Space Center
Cocoa Beach, Florida 32931

Melpar, Inc.
3000 Arlington Boulevard
Falls Church, Virginia 22046

November 1965

TABLE OF CONTENTS

		Page
1.	INTRODUCTION	4
2.	GENERAL	5
	2.1 UV Results	5
	2.2 IR Results	9
3.	CONCLUSIONS	11
4.	INSTRUMENT DESCRIPTION	12
5.	CALIBRATION STANDARDS AND PROCEDURES	15
	5.1 Wavelength Calibration	15
	5.2 Radiation Calibration	15
	5.2.1 Basic Radiance Calibration	19
	5.2.2 Attenuator Calibration	19
	5.2.3 Focal Index Calibration	24
	5.2.4 Final Correction	24
6.	DATA COLLECTION	28
7.	DATA REDUCTION	30
APPENDIX A -- Natural Ultraviolet Irradiance at Sea Level		A-1
APPENDIX B -- Spectral Radiance Standards		B-1

LIST OF ILLUSTRATIONS

Figure		Page
1	Ultraviolet Spectra	6
2	Infrared Spectra	7
3	Left View of Spectrophotometer	13
4	Right View of Spectrophotometer	14
5	Wavelength Calibration, Ultraviolet to Visible	17
6	Wavelength Calibration, Visible to Infrared	18
7	UV Standard Lamp Characteristic	20
8	IR Standard Lamp Characteristic	21
9	UV Calibration Factors	22
10	IR Calibration Factors	23
11	Focal Correction Factor	26
12	Calibrator Box	27
13	Recorder Calibration, UV Work	32
14	Recorder Calibration, IR and UV Work with Preamplifier	33

LIST OF TABLES

Table		Page
1	Spectrum Lines for Calibration Curves	16
2	IR and UV Attenuator Calibration	25
3	Spectral Data Obtained at KSC	29

1. INTRODUCTION

This report covers the results of Task D of Contract No. NAS10-2009, Hazards Monitoring Study, as amended, between NASA-KSC and Melpar, Inc. The purpose of the task was to measure the spectral radiance of the background at Cape Kennedy and the spectral radiance of a hydrogen flame in air. The spectral regions of interest lie between 2000 angstroms and 3.0 microns, with the visible region (0.4 to 0.7 microns) excluded.

The remaining three tasks under this contract are covered in three additional separately bound final reports. They are:

Volume I, Task A -- Sensor Selection and Location for Apollo Fuel Transfer and Tanking System.

Volume II, Task B -- Ultrasonic Leak Detectors for Cryogenics and Gases.

Volume III, Task C -- Data Display and Transmission System.

2. GENERAL

The results of the ultraviolet spectrum measurement are presented in figure 1, and those of the infrared spectrum are shown in figure 2. The targets which were selected for measurement are considered representative of the background radiation environment at KSC in which a hydrogen flame detector would have to operate.

2.1 UV Results

The daytime data, (curves 1 to 8 of figure 1) indicate that the energy in the band 3200 to 4000°A is nearly constant with wavelength and varies over approximately a decade as a function of the object viewed. The brightest object viewed was the sky, about 10° from the sun (curve 3). A bright reflection from a stainless steel pipe (curve 5) was nearly identical. The loss of some fine detail is noticeable in curves 4, 7, and 8, which were taken at twice the slit width used in other runs. The curves are shown dashed at wavelengths shorter than 3050°A to indicate that the data has been modified. Tests performed during the data reduction effort revealed that the monochrometer overlapped a portion of the visible spectrum and transferred it spuriously onto the ultraviolet range. The effect was significant when the ultraviolet energy was a few orders of magnitude less than the visible energy. The solar spectra was therefore extended into the shorter wavelength range by comparing the valid spectra between 3050°A and 4000°A with normalized values from appendix A.

Curve 9 is the spectrum of a hydrogen flame burning in air. The flame measured 1 inch in diameter and 6 inches long, which is more than sufficient to fill the field of the viewing instrument at the test distance of

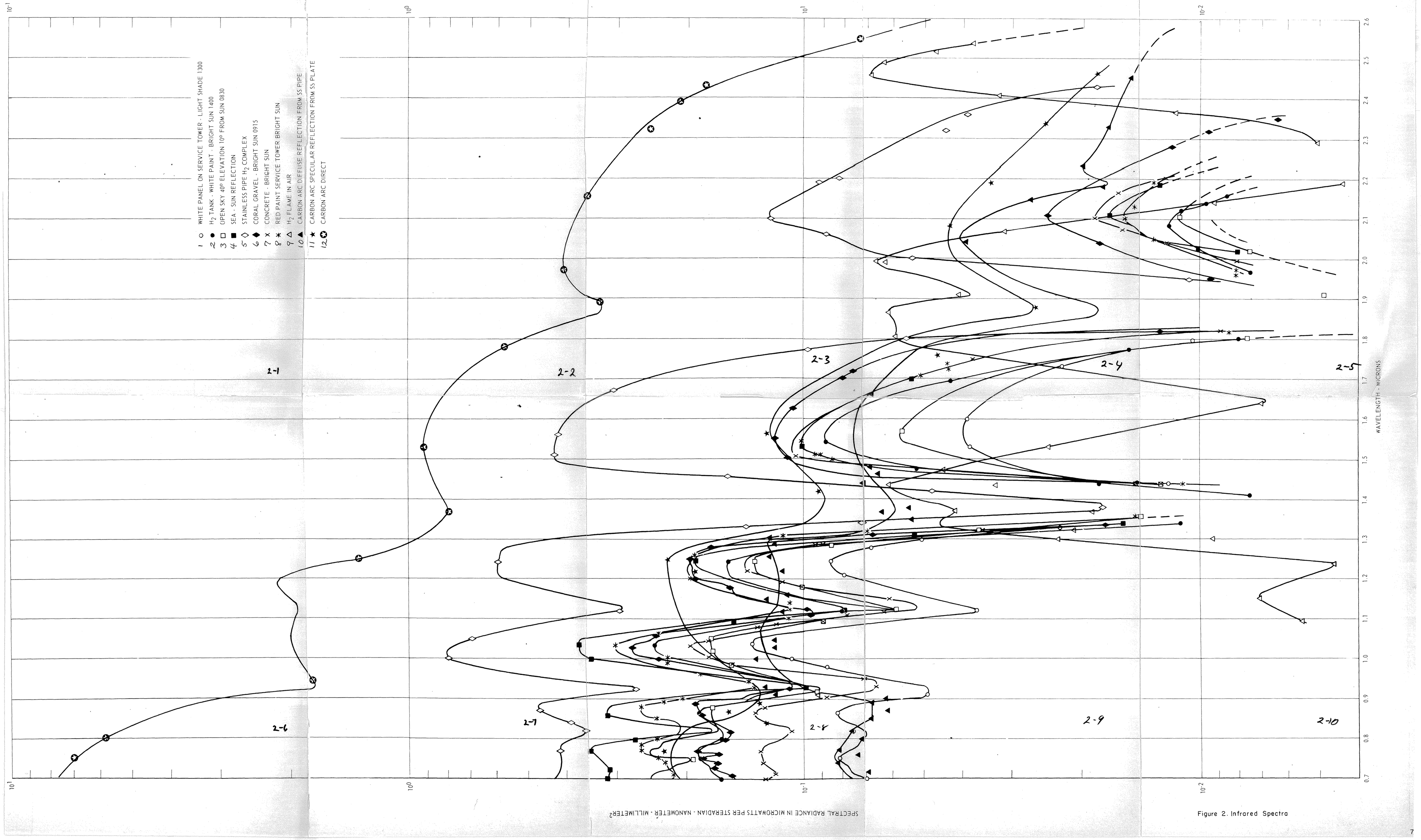

Figure 2. Infrared Spectra

GRAPH X

E3904

SPECTRAL RADIANCE IN MICROWATTS PER STERADIAN-NANOMETER-MM^2 OF SOURCE

10^2
10^1
10^0
10^{-1}
10^{-2}
10^{-3}
10^{-4}
10^{-5}
10^{-6}
10^{-7}

2300 2500 3000 3500 4000

WAVELENGTH IN ANGSTROMS

1 ○ WHITE PANEL ON SERVICE TOWER - LIGHT SHADE 1300
2 ● H_2 TANK - WHITE PAINT - BRIGHT SUN 1400
3 □ OPEN SKY 40° ELEVATION 10°FROM SUN 0830
4 ■ SEA - SUN REFLECTION
5 ◇ STAINLESS PIPE H_2 COMPLEX
6 ◆ CORAL GRAVEL - BRIGHT SUN 0915
7 X CONCRETE - BRIGHT SUN
8 ✳ RED PAINT SERVICE TOWER BRIGHT SUN
9 △ H_2 FLAME IN AIR
11 ★ CARBON ARC SPECULAR REFLECTION FROM SS PLATE
12 ✪ CARBON ARC DIRECT

Figure 1 Ultraviolet Spectral Radiance

50 feet. A 0.060 ID stainless tube was used as an orifice; no pre-mixing was employed. Only the most prominent hydroxyl bands, those near 3100°A, were sufficiently strong to reach the threshold of detectability and these are nearly 3 orders of magnitude below the brighter solar background. Much weaker bands are known to exist near 2800°A, but were not observed.

The use of an ultraviolet flame detector between 3000 and 4000°A in the presence of a solar background appears to be quite impractical from a radiant emission standpoint, although other effects, such as background chopping, or scintillation caused by changes in the refractive index of the heated gases, may yet permit detection. The signal available at wavelengths shorter than 3000°A is so weak that development of a detection system in this region is reduced to the development of a detector-filter combination, which is truly "solar blind." The data suggest that a solar rejection factor of at least 10^7 is necessary. Available information[1] indicates that no filters are reliably available that would permit conventional phototubes to be successfully employed. This reference indicated, however, that a Geiger-Mueller tube, peak sensitivity at 2200°A, did respond to thermal radiation from a high pressure hydrogen flame, while the response to sunlight was essentially zero.

Curves 11 and 12 are the spectra of a 150-ampere carbon arc searchlight with a 60-inch mirror, such as is used at KSC. Curve 11 was obtained by viewing the specular reflection of the searchlight from a flat stainless

---

1. Research Leading to the Development of a Hydrogen-Air Fire and Explosion Detection System for Aerospace Vehicles. Tech Report AFAPL-TR-65-33, DDC 448-50-1091, July 1965.

steel plate. The searchlight was 70 feet from the plate, the monochrometer 90 feet from the plate, and the angle between the searchlight beam and the monochrometer line of sight was 60°. Curve 12 was obtained on the axis of the searchlight, looking directly into the light from a distance of 90 feet. The temporal variations of the arc are so great that no fine spectral structure is reliably discernible; therefore, a line is used to outline the radiance levels. The short wavelength limit is defined by the characteristics of the glass in the searchlight, but was not observed due to the overlapping indicated above. With the exception of direct observation of the arc, the background provided by the arc between 3000 and 4000°A is no more severe than sunlit backgrounds.

2.2 IR Results

The daytime data, curves 1 to 8, figure 2, indicate that water vapor is the only significant absorber in this region. The overall variation in infrared radiance between various targets is of the same order of magnitude as in the ultraviolet, but the order of brightness is somewhat rearranged. The stainless pipe is again highly reflective. With increasing wavelength, the sky radiance decreases more rapidly than is the case with other targets.

Curve 9 shows the strong water emission bands of the hydrogen flame. The bands near 1.87 μ and 2.5 μ are of special interest. These findings are at variance with reference 2, for the peak spectral radiance measured in the infrared region is approximately 600 times that measured in the ultraviolet region. In terms of power, the additional width of the infrared water lines as compared to the ultraviolet lines provide at least a

2. Hydrogen Fire Detection -- NASA 52-006, March 1965.

factor of 10 increase in available signal power, so that perhaps 6000 times as much power appears to be available in the 1.87 μ water band as in the 3100°A hydroxyl bands.

Of more significance is the signal-to-background power ratio implied by these curves, which is at least 10 to 1 in the band under observation. The infrared bands are also of interest because they fall into the hardware and technology of lead sulfide-and-glass, which is well developed. On the other hand, present technology in imaging devices is better developed in the near ultraviolet region than in the infrared. The data also suggest that a usable signal might be obtained on the long wavelength skirt of the 2.7 μ water band, say at 3.1 μ. Although this is a region where components are slightly more expensive, the advantage of the reduction of sensitivity to glass-enclosed artificial lights might well outweigh the cost consideration.

The arc lamp spectra (curves 10, 11, and 12) are not well detailed due to temporal variations. Curve 10, taken at KSC compares well with curve 11, taken at Melpar. The KSC data were obtained at similar distances, but the reflecting target was a stainless pipe rather than a flat plate. The direct arc, curve 12, shows far more energy than the other observations in the water absorption bands. An infrared detector would, indeed, be ineffectual in the presence of a nearby arc lamp if it were required to look directly into it or at a bright reflection.

3. CONCLUSIONS

a. The daytime ultraviolet background is several orders of magnitude above the brightest hydroxyl lines which occur near 3100°A. A system which seeks to detect, by virtue of radiant contrast in this spectral region, a small flame in a background of strong sunlight appears infeasible.

b. Quantitative measurements of the radiation from hydrogen-air flames at wavelengths shorter than 3000°A were limited by the detection limits of the system as well as by an overlapping of the visible spectrum, which precluded radiant calibration in this region.

c. The infrared data taken indicate that hydrogen flame detection in the presence of a bright natural background is feasible in the atmospheric water absorption bands.

4. INSTRUMENT DESCRIPTION

The monochrometer used in the spectrophotometer that was assembled for these measurements was a standard instrument removed from a Perkin-Elmer Model 13 spectrophotometer. A fused silica prism which is available for this device was installed and an auxiliary photomultiplier detector mount attached. A type 1P28 photomultiplier was used for measuring ultraviolet radiation and a lead sulphide detector used for the infrared work. A Melpar built motor-driven mechanical chopper (210 cps) was mounted in front of the entrance slit and a retractable reflex viewing periscope was attached behind the entrance slit to permit positive identification of the target. To enhance portability and reliability, a transistor amplifier and attenuator was also built. Figures 3 and 4 show the left- and right-hand views of the spectrophotometer as well as some of the auxiliary equipment used.

A Newtonian telescope with a 6-inch diameter and 48-inch focal length objective was fitted to the monochrometer. The larger end of the telescope (figure 4) contains a crank handle and a precision slide for moving the objective lens, permitting the telescope to be focused from 50 feet to infinity.

Auxiliary equipment includes the necessary detector bias supplies and amplifiers to provide a signal level suitable for recording on a Precision Instrument Company Series PS200A seven-channel tape recorder. An oscilloscope and a logarithmic a voltmeter (Ballantine Model 302C) were used for monitoring recording levels.

The equipment was mounted on a reinforced plywood base fixed to an electrically driven antenna mount for ease of pointing.

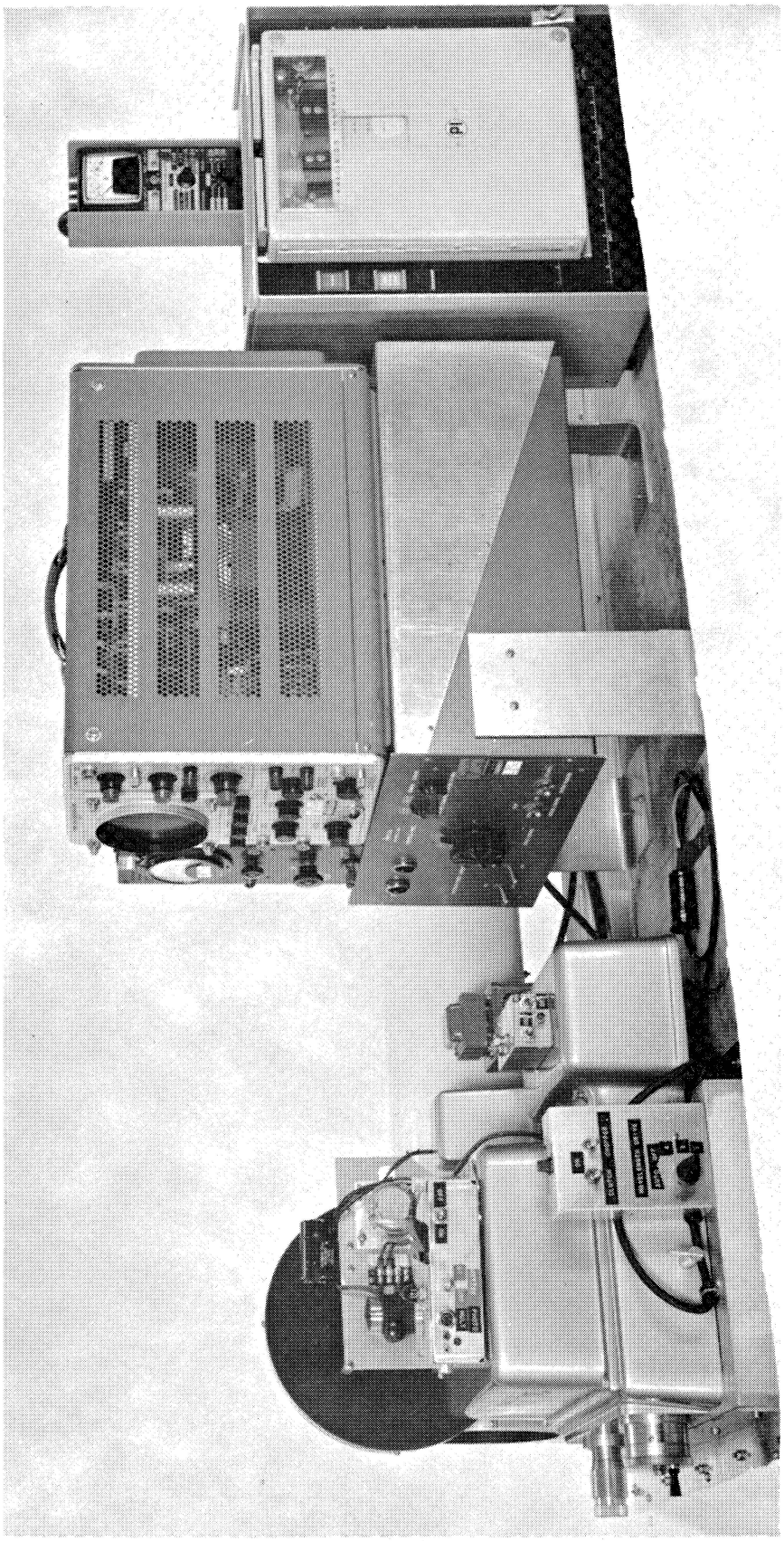

Figure 3. Left View of Spectrophotometer

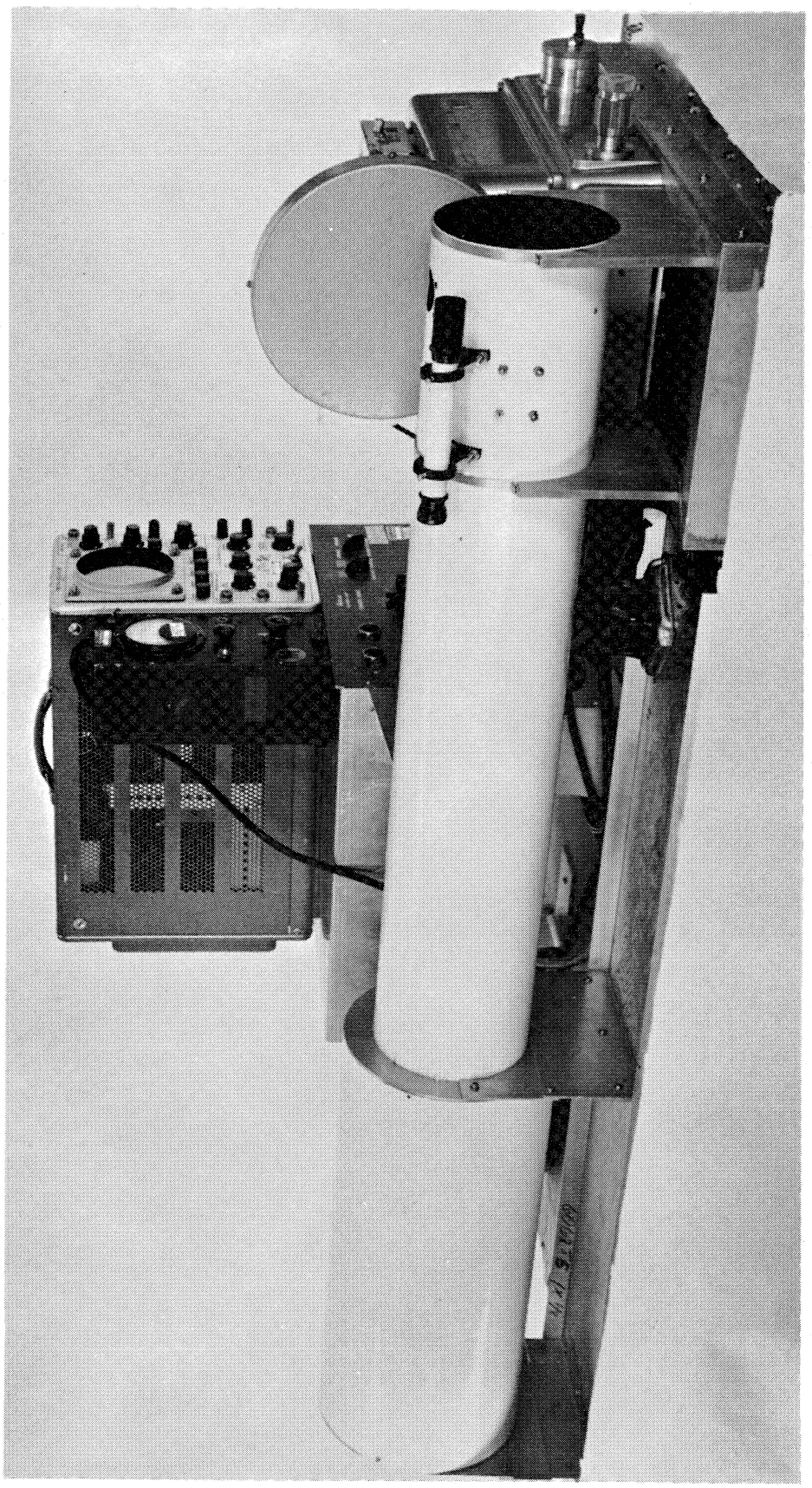

Figure 4. Right View of Spectrophotometer

5. CALIBRATION STANDARDS AND PROCEDURES

The calibration standards used were a General Electric H100-A4 mercury source for wavelength calibration and an Eppley Laboratories calibrated standard of spectral radiance, serial No. EPI - 1047, for radiance calibration. (See appendix B.) Calibration procedures followed are described below.

5.1 Wavelength Calibration

The Model 13 monochrometer does not have a direct reading wavelength scale, but has a drum that indicates lead-screw position. The starting point for wavelength calibration was the yellow mercury doublet at 576.96 and 579.07 millimicrons. Table 1 lists the lines used in determing the calibration curves shown in figures 5 and 6. The lines between 205.29 to 1128.7 are those furnished by Mellon[1] and those from 1128.7 to 2325.3 are taken from the Handbook of Chemistry and Physics.[2] The three points near 3.3 microns were determined using a Beckman wavelength calibrator[3] (a polystyrene film) and by comparison with measurements taken with a Beckman IR5 spectrophotometer.

5.2 Radiation Calibration

The objective of using the several radiance calibration factors was to permit a comparison between the object and a standard source by compensating for each field-use parameter which was not identical to that used

1. Analytical Absorption Spectroscopy, Absorptimetry and Colorimetry, Edited by M. G. Mellon, Purdue University. Copyright 1950 by John Wiley & Sons, Inc., p 206.

2. Handbook of Chemistry and Physics, 31st edition, Copyright 1949 by Chemical Rubber Publishing Co., Cleveland, Ohio., pp 2105 and 2179-2180.

3. Beckman Scientific and Process Instruments Division, Fullerton, Calif.

TABLE 1

SPECTRUM LINES FOR CALIBRATION CURVES

Drum Number	Wavelength in Millimicrons
2078.0	205.29
2010.0	222.47
1971.5	232.32
1964.0	235.25
1945.0	239.95
1895.0	253.63
1870.0	260.32
1840.0	269.95
1814.0	275.97
1788.0	284.78
1773.0	289.36
1760.0	292.54
1742.0	296.73
1721.0	302.25
1685.0	312.37
1683.0	313.16
1620.0	334.15
1550.0	365.01
1505.0	390.01
1484.0	404.66
1480.0	407.78
1443.0	435.83
1394.0	491.60
1357.0	546.07
1340.0	576.96
1339.0	579.07
1296.0	690.72
1226.0	1014.0
1208.0	1128.7
1174.0	1357.0
1172.0	1367.3
1168.0	1395.0
1147.0	1529.5
1120.0	1692.1
1118.0	1707.3
1114.0	1711.0
1100.0	1833.3
1072.0	1970.1
998.0	2325.3
775.0	3304.0
748.5	3355.0
738.0	3420.0

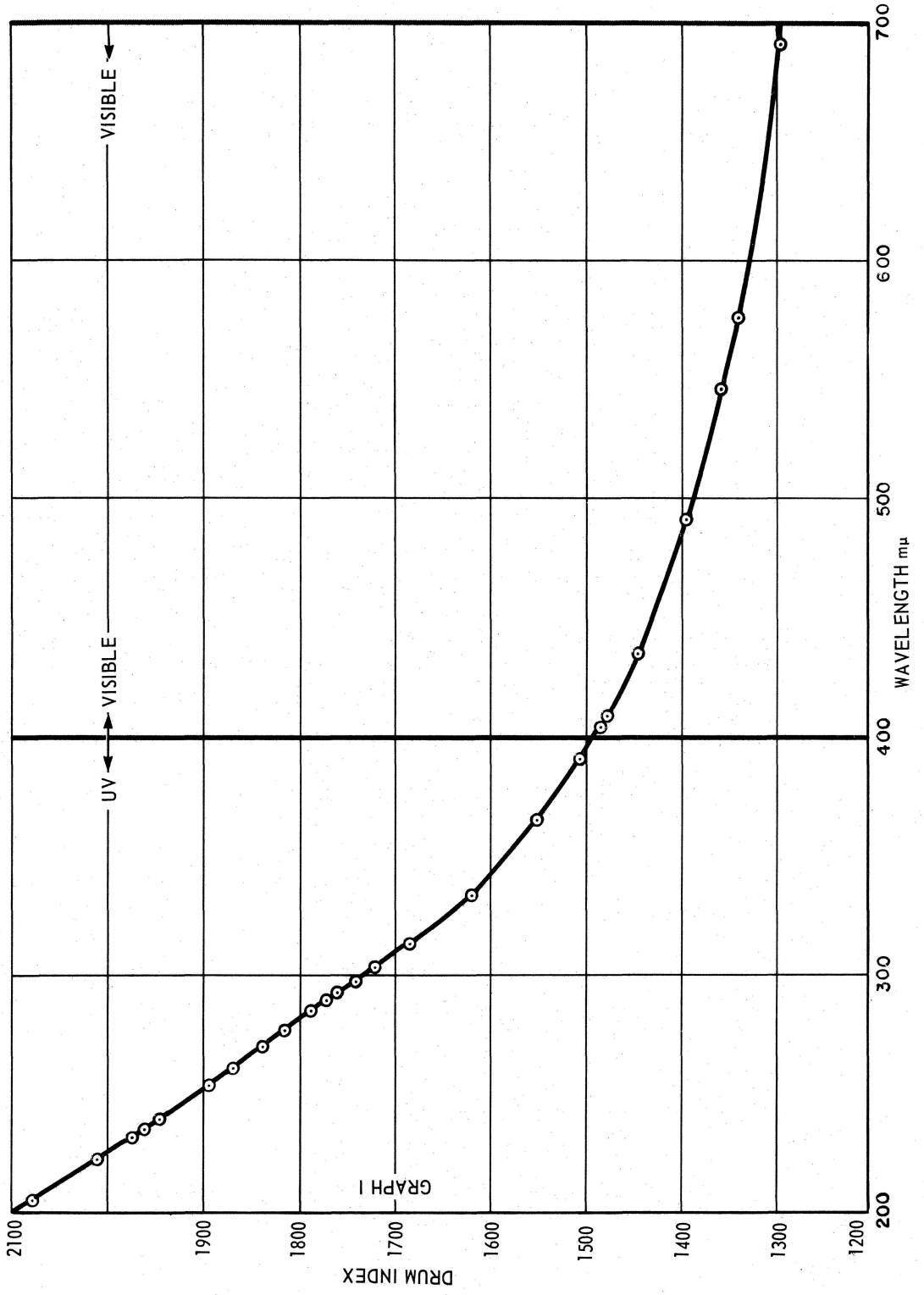

Figure 5. Wavelength Calibration, Ultraviolet to Visible

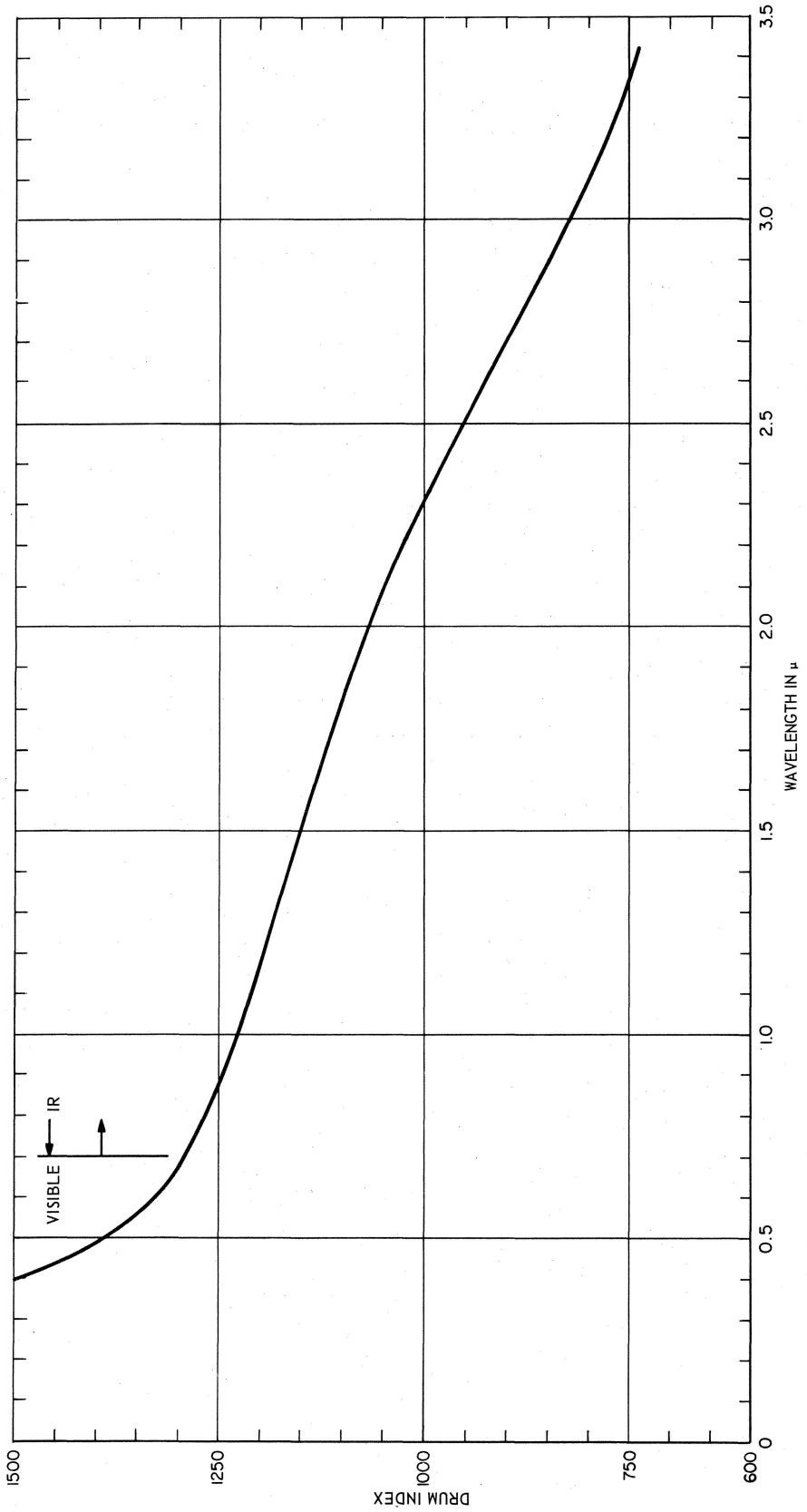

Figure 6. Wavelength Calibration, Visible to Infrared

during laboratory measurement of the standard source. An arbitrary electrical reference is assigned to a radiance value and corrections are made to object observations to return to this reference by the use of calibration curves. The calibration procedures used are described below.

5.2.1 Basic Radiance Calibration

This calibration was accomplished by viewing the standard source at various slit widths and plotting the signal output as a function of wavelength to the same scale factor as a plot of standard source radiance, thus establishing an arbitrary electrical reference. Typical curves thus obtained are shown in figures 7 and 8. The difference between the radiance curve and the signal curve is then plotted as a calibration curve, as in figures 9 and 10. In the region from 250 mμ to 2600 mμ, the major uncertainty associated with the calibration source in the development of the calibration curve is the correction made to this difference to allow for the reflectivity of a large (40-inch diameter, 168-inch focal length) collimating mirror used in conjunction with the standard source to provide a larger image at the entrance slit than was possible by direct viewing of the source with the 50-foot focusing limit of the telescope. Outside of these spectral regions, the standard source is not calibrated and an extension of the radiance curve was made. As a result, in the ultraviolet range, some uncertainty exists, and the radiance curve was estimated by fitting a modified blackbody curve to the existing data.

5.2.2 Attenuator Calibration

Because the expected signal range exceeded the dynamic range of the tape recorder, the detector amplifier was fitted with appropriate signal

E-3908

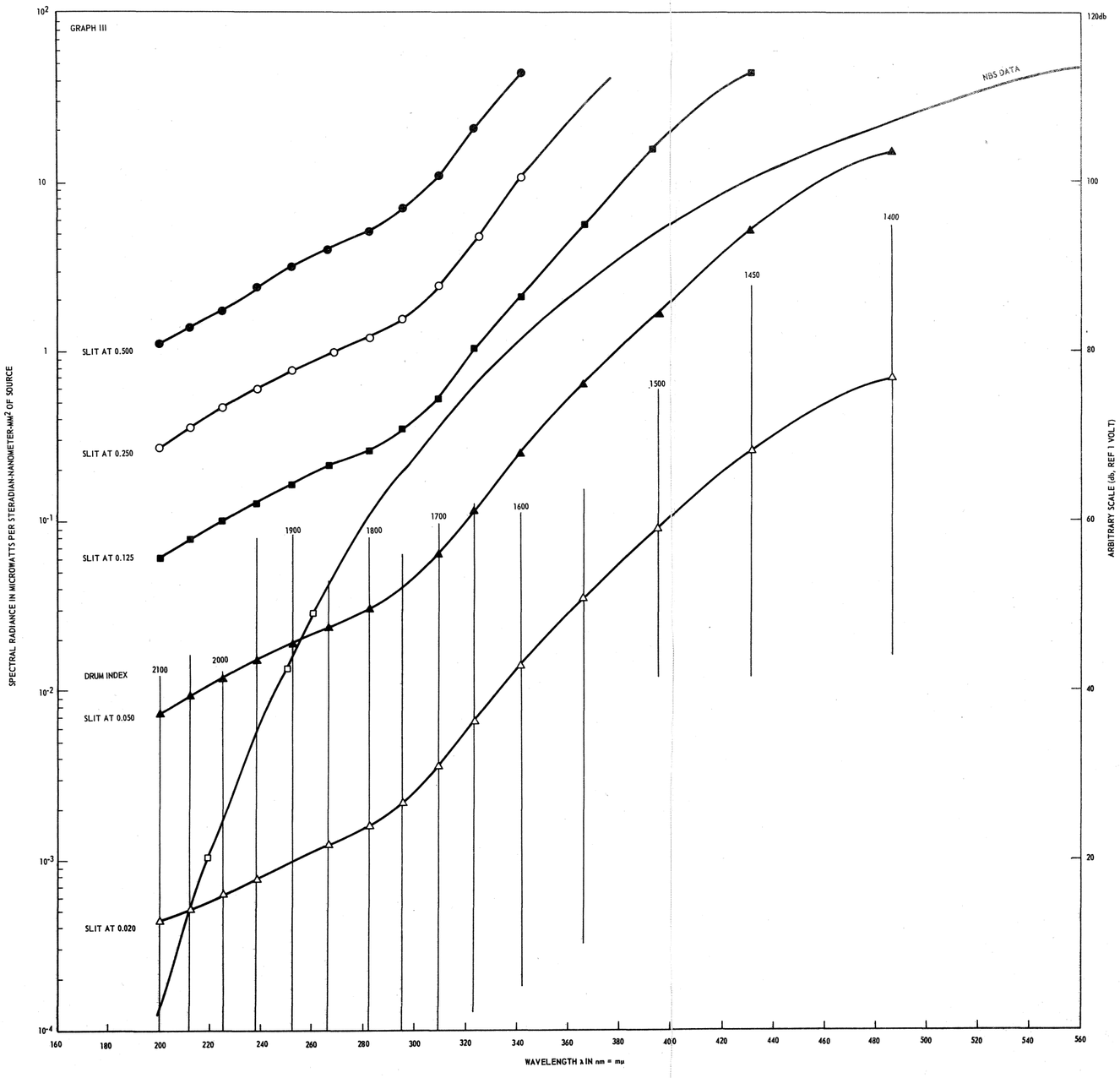

Figure 7. UV Standard Lamp Characteristic

20 0 (2)

E3909

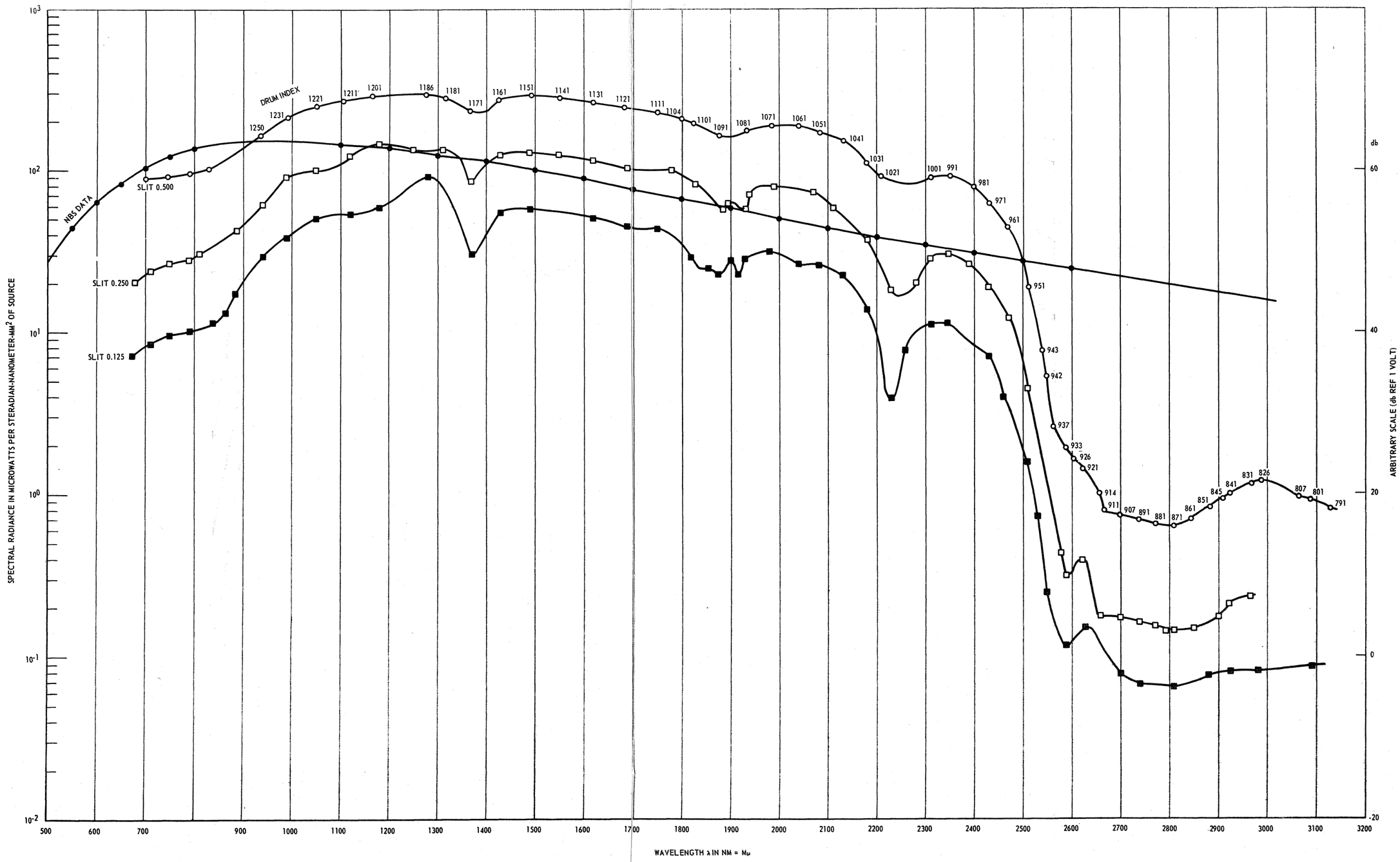

Figure 8. IR Standard Lamp Characteristic

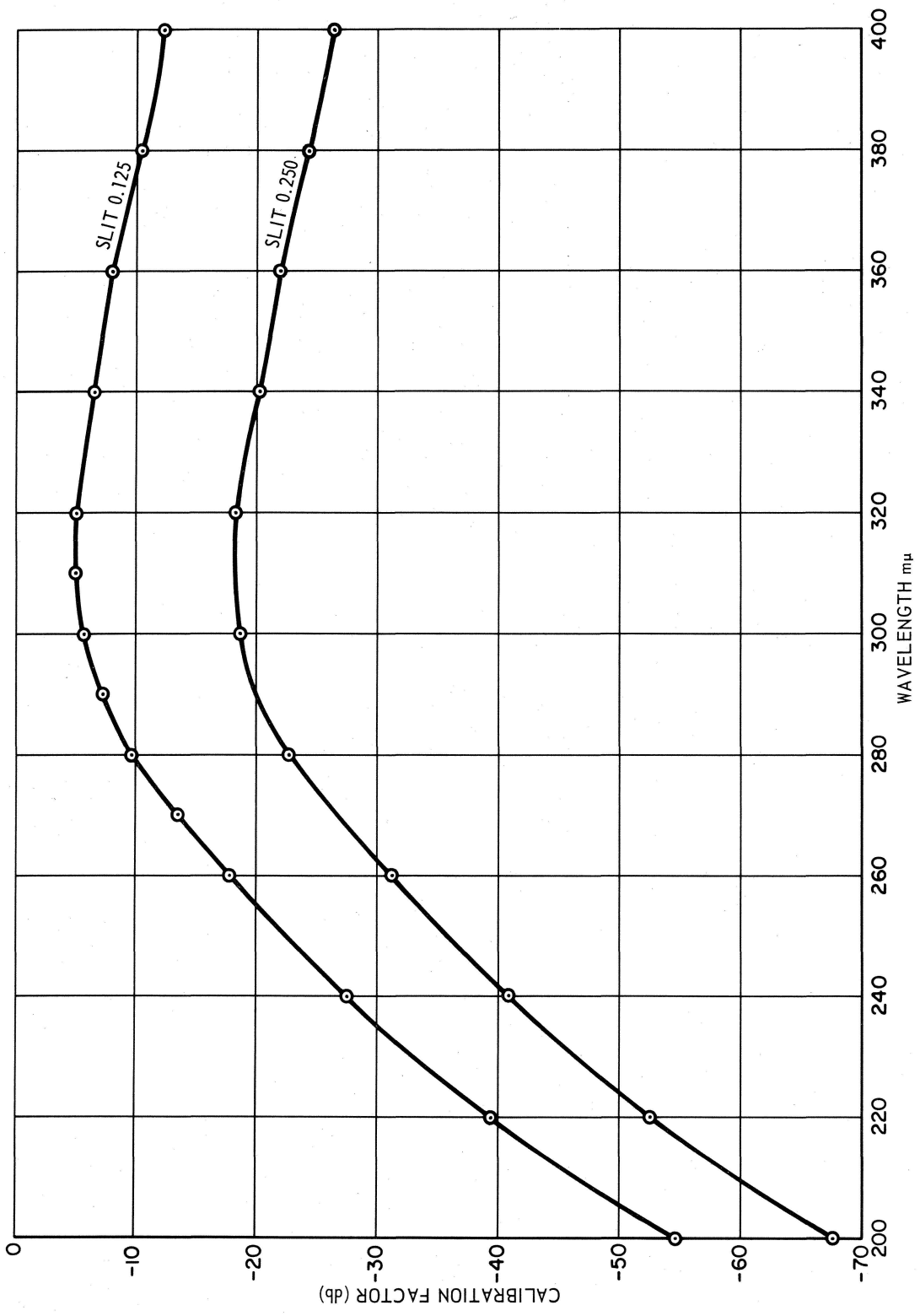

Figure 9. UV Calibration Factors

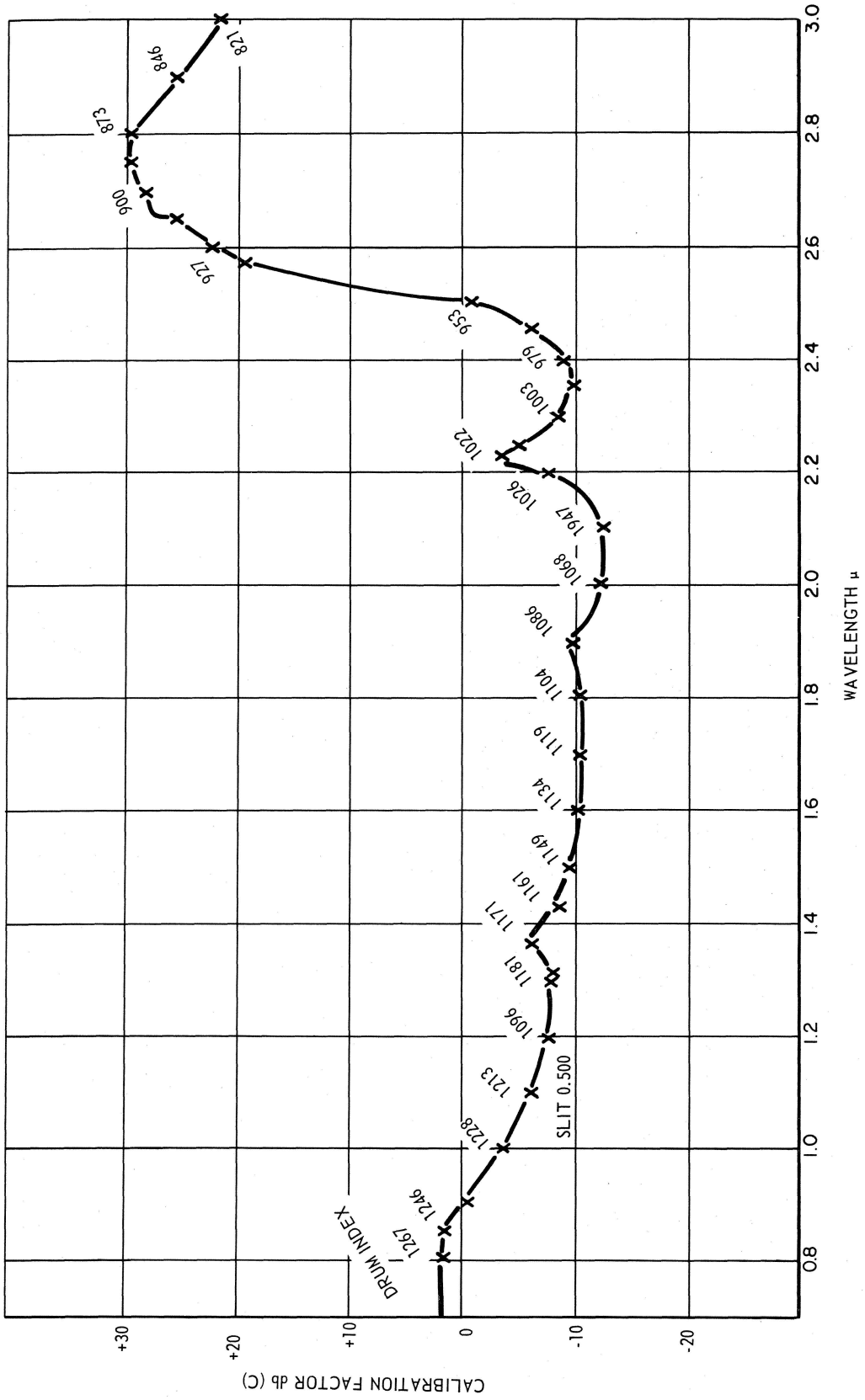

Figure 10. IR Calibration Factors

attenuators. The values shown in table 2 were obtained by varying the radiant energy input to the appropriate detector and measuring the detected signal voltage at various attenuator positions in the same manner that target observations would be made.

5.2.3 Focal Index Calibration

An arbitrary position scale (focal index) was fixed to the focusing adjustment and a correction factor was obtained by measuring the signal change that occurred when the objective lens was moved throughout its range while looking at a large uniform diffuse target. The result is shown in figure 11. The focal index is arbitrarily taken as 1.1 at infinity focus with 0.0 db correction assigned at infinity, since this was the position at which the radiance calibration was performed.

5.2.4 Final Correction

In order to ensure that no severe mechanical stress, which may have been imposed by shipping the equipment to KSC, had changed the optical alignment, thus causing a shift in radiant and/or spectral calibration, the standards were installed in a calibrator box, figure 12, and transported to KSC to provide means of making a simple check on the entire system. A check of calibration at KSC confirmed that no significant mechanical change had occurred.

TABLE 2

IR AND UV ATTENUATOR CALIBRATION*

Calibration of Attenuator for Infrared Region

Attenuator	Preamplifier	Correction (db)
P1	in	0.0
P2	in	23.0
P3	in	36.2
P4	in	55.5
P5	in	66.4

Calibration of Attenuator for Ultraviolet Region

Attenuator	Preamplifier	Correction (db)
P1	in	0.0
P2	in	26.0
P3	in	39.6
D1	out	47.6
D2	out	61.3
D3	out	80.6
D4	out	100.8
D5	out	111.0

*Reference level: 1 volt = 0 db.

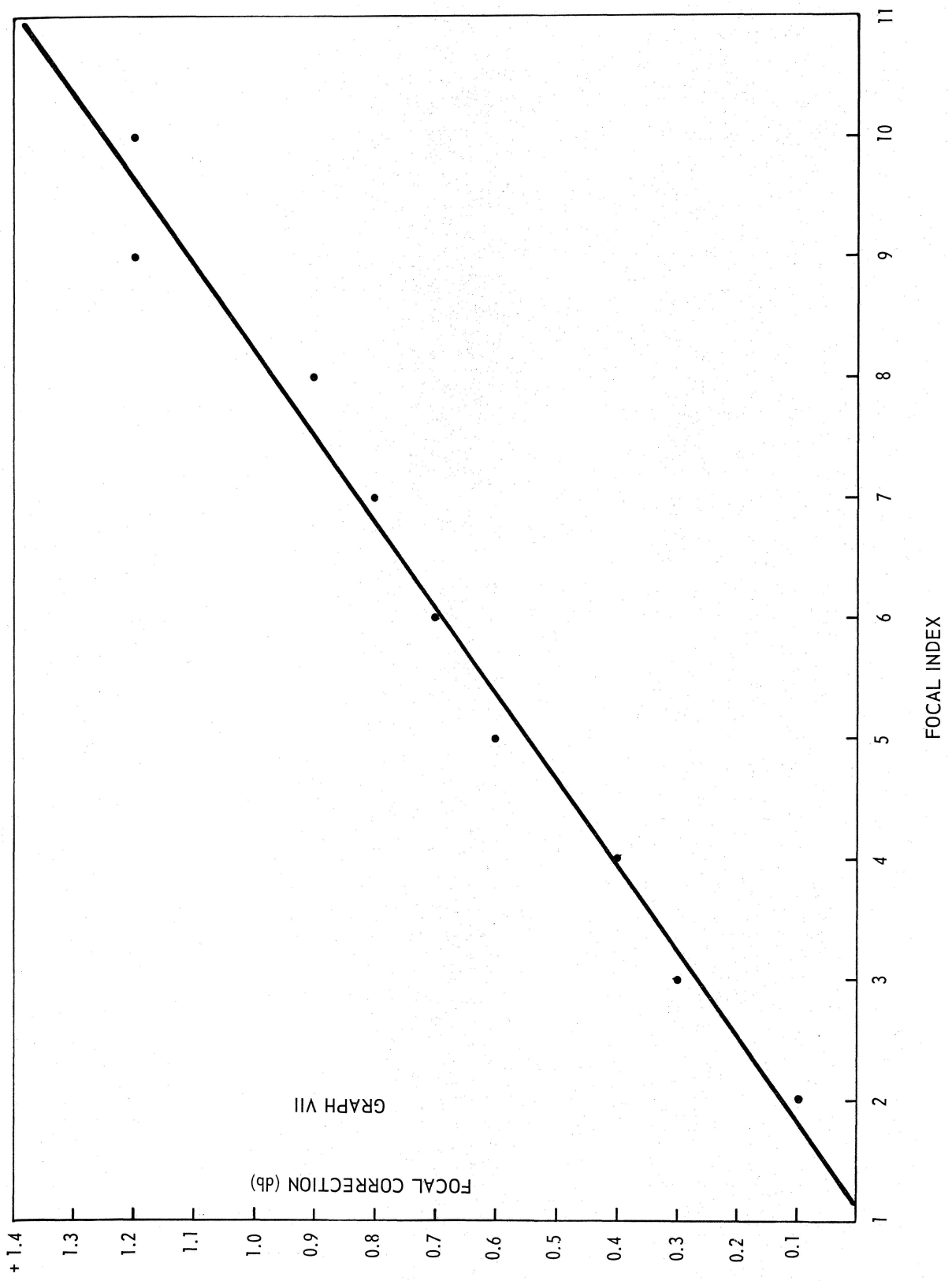

Figure 11. Focal Correction Factor

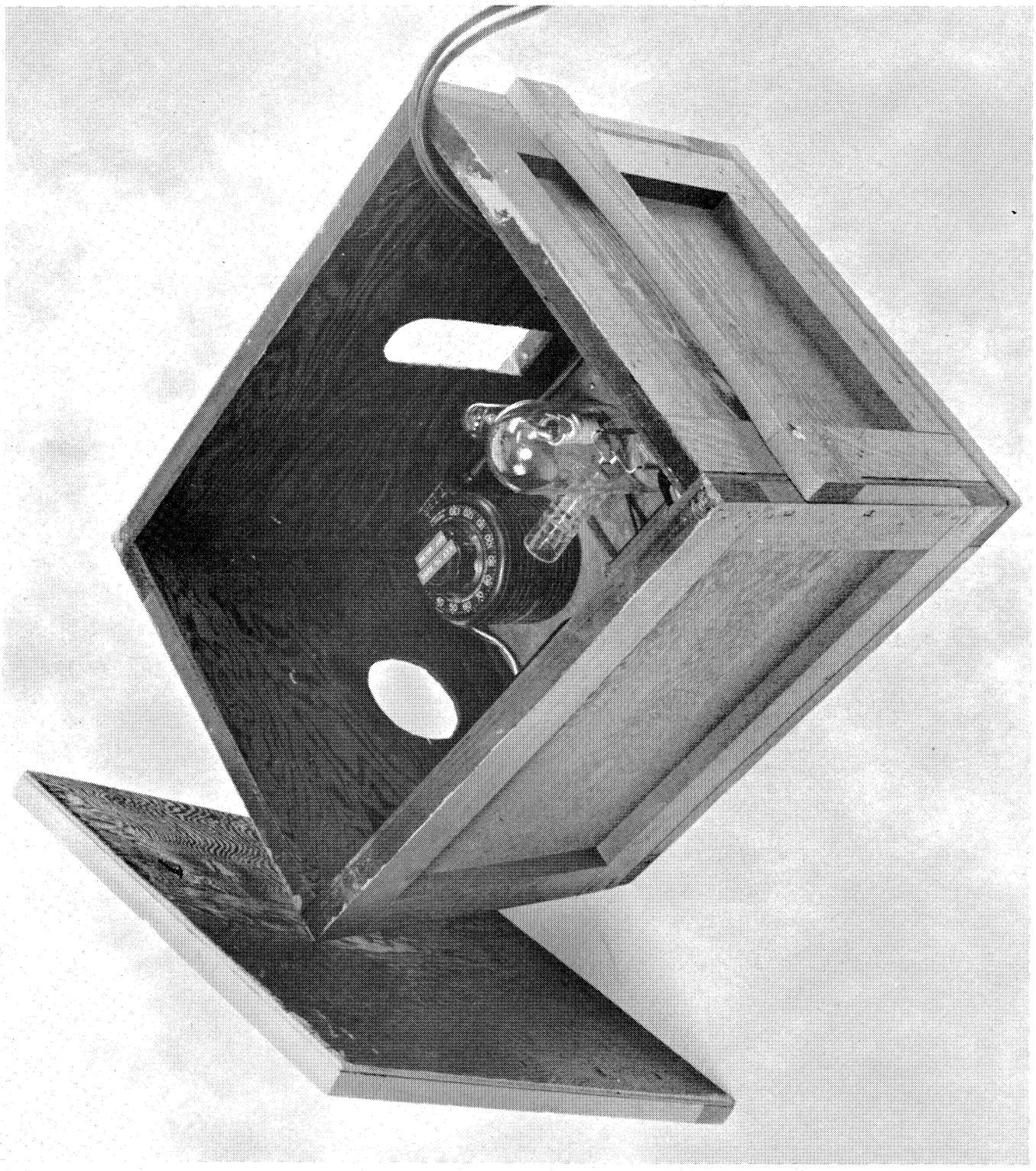

Figure 12. Calibrator Box

6. DATA COLLECTION

At Kennedy Space Center within Launch Complex 37, the monochrometer was pointed at a number of targets which were judged to be typical of the background that would be seen by hydrogen flame detectors which might be used there. These targets include a white panel on the service tower, a specular reflection of the sun from the large, white, spherical liquid hydrogen storage tank, the reflection of the sun from the ocean at low angles about two hours after sunrise, a white coral gravel roadway, the open sky at an elevation angle of 40° when the sun was at an elevation of 50°, a stainless steel pipe leading to the spherical liquid hydrogen tank, the unpainted concrete walkway in the vicinity of the LH_2 tank, and red paint on the service tower.

For the KSC runs, the monochrometer was mounted inside a large truck open-ended at the back and vibration-stabilized by two jacks symmetrically placed under the truck base. Approximately half of the KSC runs were made from the top of a photography station, the highest and best ground vantage point inside LC 37; the other half were made near the liquid hydrogen tank, in proximity to the service tower. All of the day runs were taken between the early morning and early afternoon when the sun was at its brightest and before clouding of the sky, which occurs almost daily at KSC in the mid-afternoon. An observation of a carbon arc searchlight was made during a night test.

In addition, spectral data were taken at Melpar using as targets a carbon arc searchlight similar to the searchlights used at KSC, and a hydrogen flame burning in air. Table 3 summarizes the runs made at KSC and stored on tape.

TABLE 3

IDENTIFICATION OF TEST RUNS

Test	Target	Data Channel	Voice Channel	Slit Width (mm)	Focal Index
A	(Recorder calibration)	7	5	-	-
IR1	Service tower - white panel	7	5	0.500	1.2
IR2	Service tower - white panel	7	5	0.500	1.2
UV1	Service tower - white panel	7	5	0.250	1.2
UV2	Service tower - white panel	7	5	0.250	1.2
UV3	Service tower - white panel	7	5	0.125	1.2
IR3	H_2 tank in sun bright spot	7	5	0.500	3.4
IR4	H_2 tank in sun bright spot	7	5	0.500	3.4
UV4	H_2 tank in sun bright spot	7	5	0.125	3.4
UV5	H_2 tank in sun bright spot	7	5	0.125	3.4
UV6	H_2 tank in sun bright spot	1	2	0.125	3.4
B	(Recorder calibration)	1	2	-	-
IR5	Sea-sun reflection	1	2	0.500	6.3
UV7	Sea-sun reflection	1	2	0.250	6.3
IR6	Coral gravel	1	2	0.500	10.2
UV8	Coral gravel	1	2	0.125	10.2
IR7	Open sky elevation 40°, sun 50°	1	2	0.500	1.2
UV9	Open sky elevation 40°, sun 50°	1	2	0.125	1.2
IR8	LH_2 tank stainless steel pipe	1	2	0.500	9.9
UV10A	LH_2 tank stainless steel pipe	1	2	0.125	9.9
C	(Recorder calibration)	3	4	-	-
IR9	Concrete	3	4	0.500	10.2
UV11	Concrete	3	4	0.250	10.2
IR10	Red paint on service tower	3	4	0.500	1.2
UV12A	Red paint on service tower	3	4	0.250	1.2

7. DATA REDUCTION

The data were recorded on magnetic tape which was returned to Melpar for analysis. Each observation consists of the analog data on one channel and a voice commentary on the other channel for collateral data.

The recorded signals were transferred to strip chart format by passing them through a high pass filter to eliminate the 60-cycle noise generated by the recorder and were detected by a Ballantine Model 302C Voltmeter. Notes were made on the chart paper of the attenuator setting and the VTVM scale. Since these "blackboxes" were not associated with the standard source measurements, recorder calibration runs which were made during the field measurements were used to transfer the arbitrary electrical reference and scale through this intermediate hardware. The recorder calibration runs were generated by varying the radiant input to the spectrophotometer in discrete steps and noting the recorder input level with voice commentary. The recorder input level was measured in the same manner that the standard source measurement was made.

The wavelength drum position was keyed to the chart paper by a marker signal injected into the data channel by a cam-operated microswitch on the drum shaft. These marks, along with the voice channel commentary, permitted the chart paper to be labeled with drum position along its time axis, which was then converted to wavelength by reference to curves such as those shown in figures 5 and 6.

The spectral intensity was computed by converting chart paper excursion to decibels by the calibration charts of figures 13 or 14, as appropriate to the detector, Ballantine ac voltmeter range and attenuator settings. The correction factors for focal index, final correction (which

are constant for any one run), the spectrally dependent calibration factor, and the attenuator calibration factor were applied to this value to yield a figure which, when plotted on the same scale as the original calibration (figures 7 and 8), yield the desired value. This procedure was carried forward for each point deemed necessary to adequately define the curve.

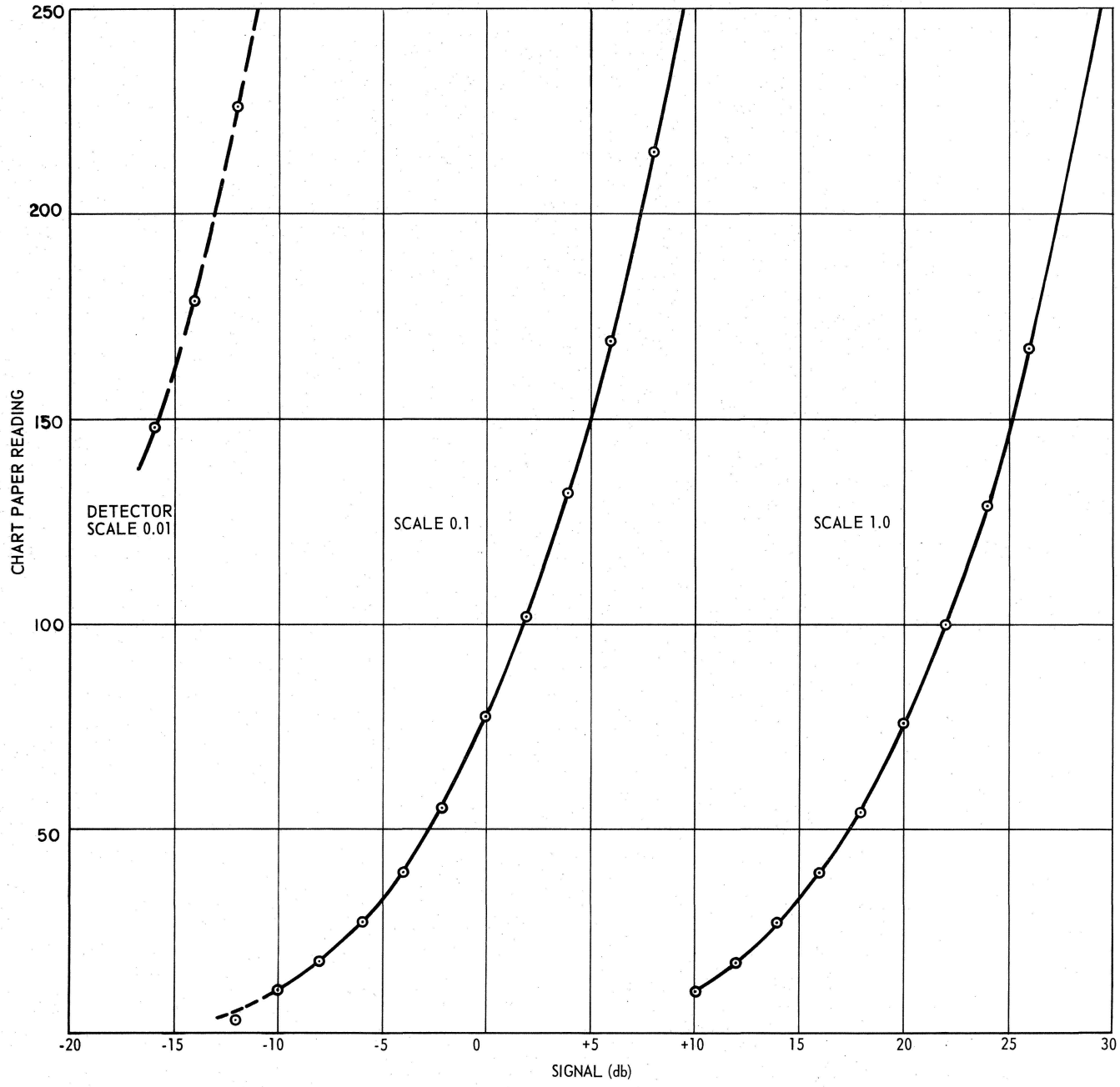

Figure 13. Recorder Calibration, UV Work

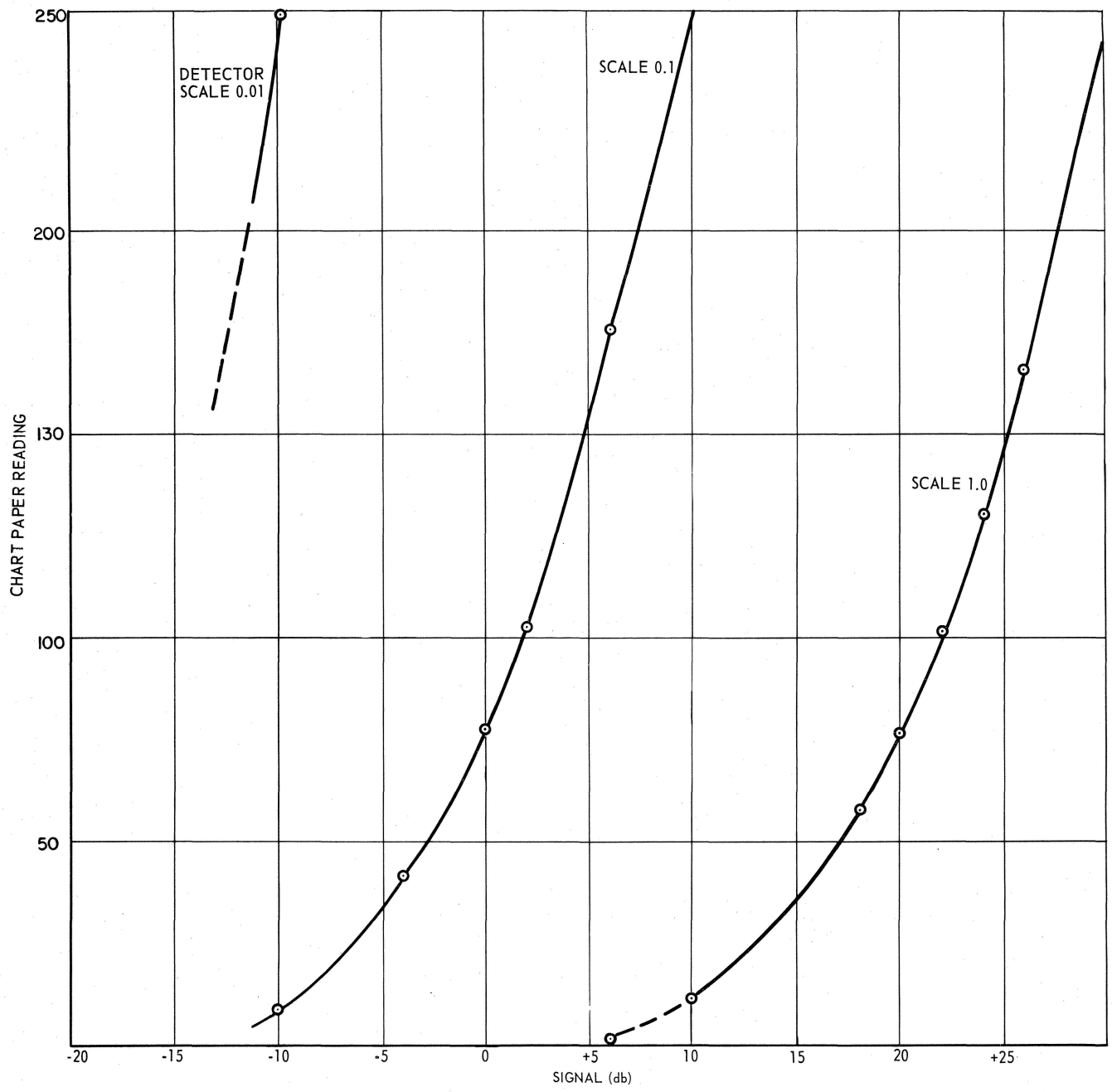

Figure 14. Recorder Calibration, IR and UV Work with Preamplifier

APPENDIX A

NATURAL ULTRAVIOLET IRRADIANCE

AT SEA LEVEL

APPENDIX A

NATURAL ULTRAVIOLET IRRADIANCE AT SEA LEVEL[1]

SUMMARY

While a brief search of the literature produced considerable experimental data on the ultraviolet irradiance of a horizontal surface at sea level for the wavelength range 0.4 to 0.3 micron, no measurements at shorter wavelengths were found. The literature demonstrates, however, that quite reliable figures can be obtained from measured irradiance above the atmosphere combined with atmospheric transmission computed on the assumption that Rayleigh scattering and absorption by oxygen and ozone determine the transmission. The maximum irradiance exists when the sun is at the zenith. For this condition, the irradiance produced by energy scattered from the sky is essentially equal to that produced by direct sunlight.

Computed irradiances for a horizontal surface, including both the direct sunlight and the sky light, are given in table A-4. The values shown are the maximum that will be obtained with the sun in the zenith and a perfectly clean atmosphere. The computed values are in satisfactory agreement with measured ones in the 0.4 to 0.3 micron region.

---

1. First published 25 Jan. 1964 by R. W. Koza, Melpar, Inc.

INTRODUCTION

A brief search of the readily available literature has not produced a reference to any direct measurement of the spectral distribution of sunlight or daylight at sea level which covers the 2000 to 3500 A region. Taylor and Kerr[1] have measured the relative spectral distribution of sunlight and daylight for clear and overcast skies, but their data are restricted to the 4000 to 7000 A region.

Stair and Johnston[2] have measured the spectral distribution of sunlight at Sunspot, New Mexico, at an altitude of 9200 feet in the spectral range 3025 to 5350 A, and have computed vertical atmospheric transmission and the spectral distribution of sunlight above the atmosphere from their data. Dunkelman and Scolnik[3] have made similar computations from data they took on Mt. Lemmon near Tuscon at an altitude of 8015 feet.

The older data are summarized in Smithsonian Tables[4] and in several books.[5,6] Again, measurements of irradiance below 2950 are not given.

The results of all of these measurements show that the vertical transmission of the total atmosphere can be computed within about 20% by assuming that the attenuation is due to Rayleigh scattering combined with absorption by ozone for the 4000 to 2500 A region.[2 3 6] At wavelengths shorter than 2500 A, absorption by oxygen must also be considered. Vertical atmospheric transmission found by this computation combined with solar irradiance data outside the atmosphere will therefore allow a reasonable estimate of solar spectral irradiance at ground level.

ATMOSPHERIC TRANSMISSION

The fraction of the incident energy transmitted over a path, ℓ, through an absorbing material is

$$T = e^{-k\ell} \qquad (1)$$

where k is the absorption coefficient per unit path length. For several absorbing materials in the same path, the quantities $k\ell$ may be added or the separate transmissions multiplied to find the total transmission. Reduced to standard temperature and pressure, the path lengths, ℓ, for the total vertical atmosphere are 1.676×10^5 cm for oxygen and 0.25 cm for ozone.[7]

The absorption coefficient of oxygen as given in table 143, page 430, in the Smithsonian Meteorological Tables,[8] is plotted in figure A-1. Values of $k\ell$ for the total vertical atmosphere are shown in column 2 of table A-1.

Figure A-2 shows the absorption coefficient of ozone as given in table 142, page 429, in the Smithsonian Meteorological Tables[8] and the more recent data of Inn and Tanaka.[9] The ozone absorption coefficient increases again above 0.44 micron starting at 0.0046 and rising to about 0.11 at 0.60 micron with some fairly strong bands in the 0.55 to 0.56 micron region. The values of $k\ell$ for ozone for the total vertical atmosphere are given in column 3 of table A-1.

The Smithsonian Meteorological tables[8] in table 144, page 431, give values of the equivalent absorption coefficient due to Rayleigh scattering. These values were computed from the equation

$$k\ell = \frac{32}{3} \pi \frac{3 (n - 1)^2}{\lambda 4} \frac{L}{N} \qquad (2)$$

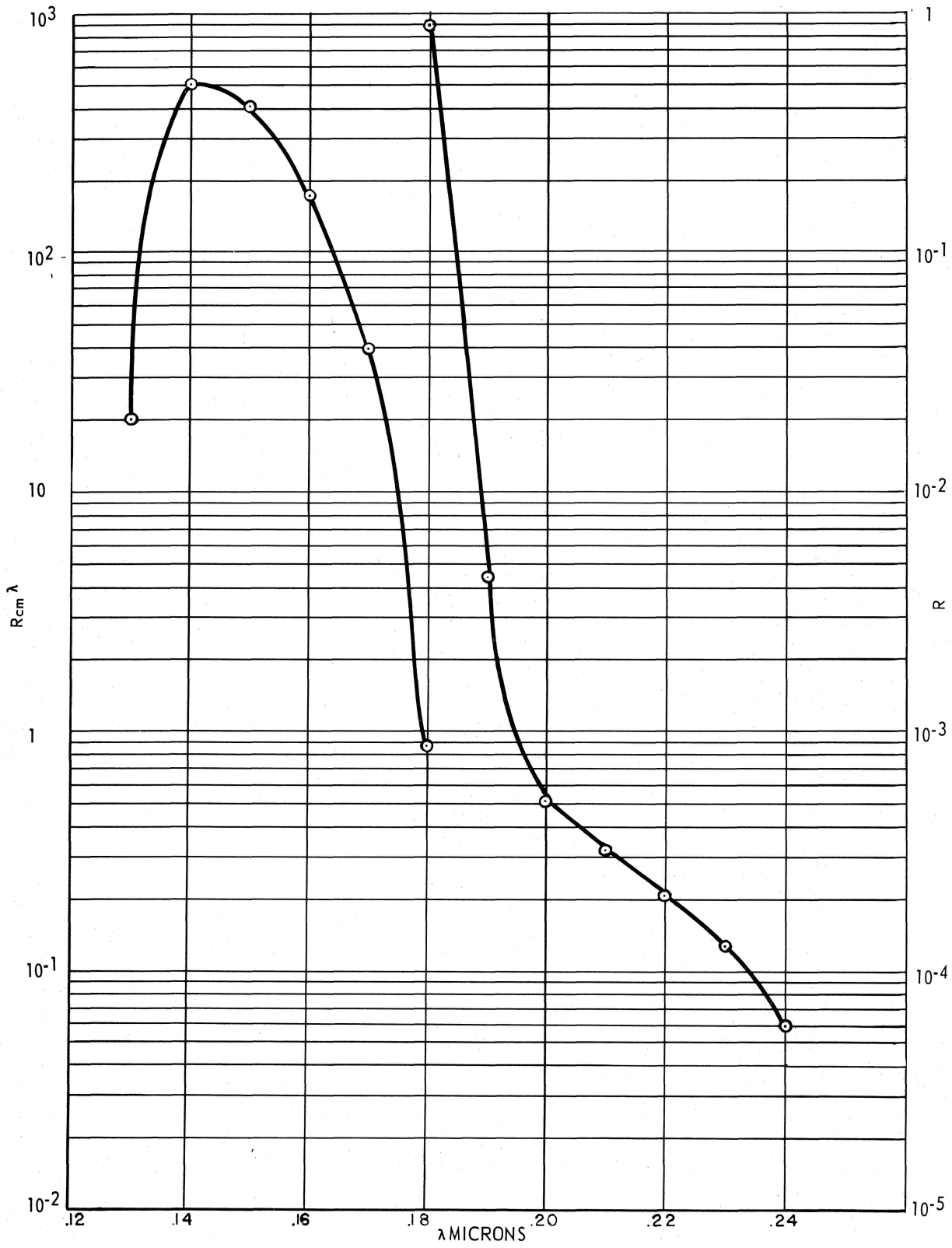

Figure A-1. Oxygen Absorption Coefficient

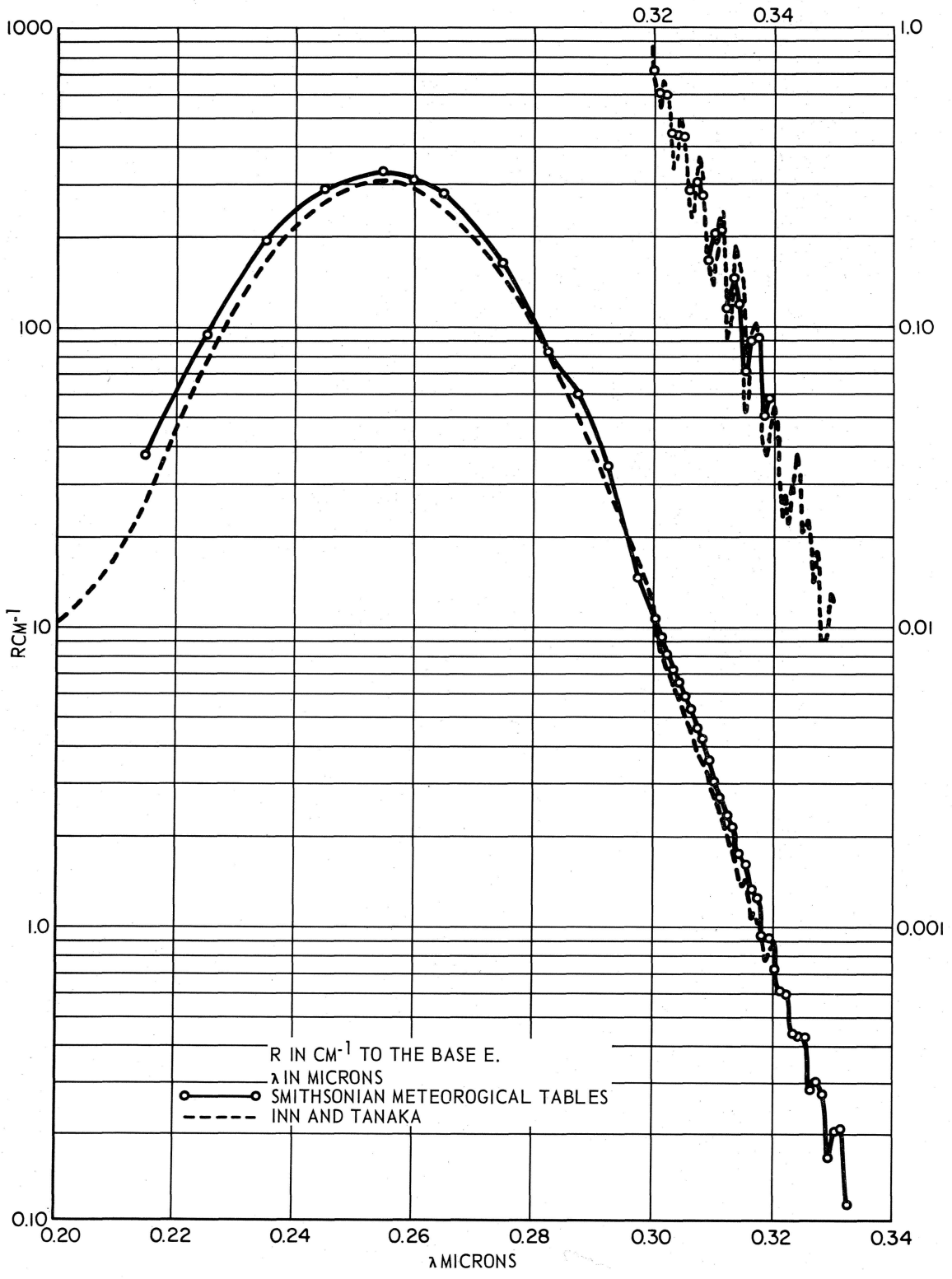

Figure A-2. Ozone Absorption Coefficient

TABLE A-1

VERTICAL ATMOSPHERIC TRANSMISSION*

λ microns	$k\ell$ oxygen	$k\ell$ ozone	$k\ell$ scatter	$k\ell$ total	T
0.20	85.5	2.59	7.21	95.3	4.090×10^{-42}
0.21	53.6	4.32	5.70	63.6	2.393×10^{-28}
0.22	35.2	11.51	4.60	51.3	5.256×10^{-23}
0.23	21.6	29.5	3.72	54.8	1.587×10^{-24}
0.24	10.1	54.0	3.09	67.2	6.537×10^{-30}
0.25		74.8	2.53	77.3	2.685×10^{-34}
0.26		73.4	2.16	75.6	1.470×10^{-33}
0.27		52.1	1.80	53.9	3.904×10^{-24}
0.28		25.9	1.56	27.5	1.140×10^{-12}
0.29		9.79	1.33	11.12	1.481×10^{-5}
0.30		2.65	1.15	3.80	0.02237
0.31		0.698	1.00	1.698	0.1830
0.32		0.219	0.873	1.092	0.3355
0.33		0.0345	0.765	0.800	0.4493
0.34		0.0113	0.674	0.685	0.5041
0.35		0.0027	0.596	0.599	0.5494
0.36			0.529	0.529	0.5891
0.37			0.472	0.472	0.6237
0.38			0.422	0.422	0.6557
0.39			0.378	0.378	0.6852

*The exponential attenuation factors $k\ell$ are for an atmosphere 7.991×10^5 cm thick with oxygen and ozone paths of 1.676×10^5 cm and 0.25 cm, respectively.

in which n is the refractive index of air at wavelength λ, L is the height of the atmosphere in cm, and N is the number of molecules per cm^3. A homogeneous atmosphere with $L = 7.991 \times 10^5$ cm, and $N = 2.70 \times 10^{19}/cm^3$ was assumed. These values of $k\ell$ are shown in figure A-3 for wavelengths from 0.8 to 0.28 micron. The points used to extrapolate the curve to 0.20 micron were computed assuming that the refractive index of air is given by

$$n\lambda^2 - 1 = 5.7149 \times 10^{-4} \lambda^2 (\lambda^2 - 0.006718)^{-1}, \qquad (3)$$

an equation which fits quite well the index values computed from the tabulated values of $k\ell$ and equation (2). The scattering coefficient is tabulated in column 4 of table A-1.

The total exponential coefficient and the resulting vertical transmission for the whole atmosphere are shown in the last two columns of table A-1. These computed transmissions for the total atmosphere are shown in figure A-4 along with the measured values of Dunkelman and Scolnik and of Stair and Johnston for the 0.3 to 0.39 micron region. The computed curve is for sea level while the experimental curves show values for the 8000- to 9000-foot altitudes. A computed curve for this altitude would be higher than the one shown due to the decrease in scattering, and the shift would be greatest at the longer wavelengths where scattering is the major loss. Thus, the agreement is acceptable.

SOLAR SPECTRAL IRRADIANCE

Johnson[10] has summarized the data on the solar spectral irradiance outside the atmosphere for the region from 0.03 to 7 microns. This summary

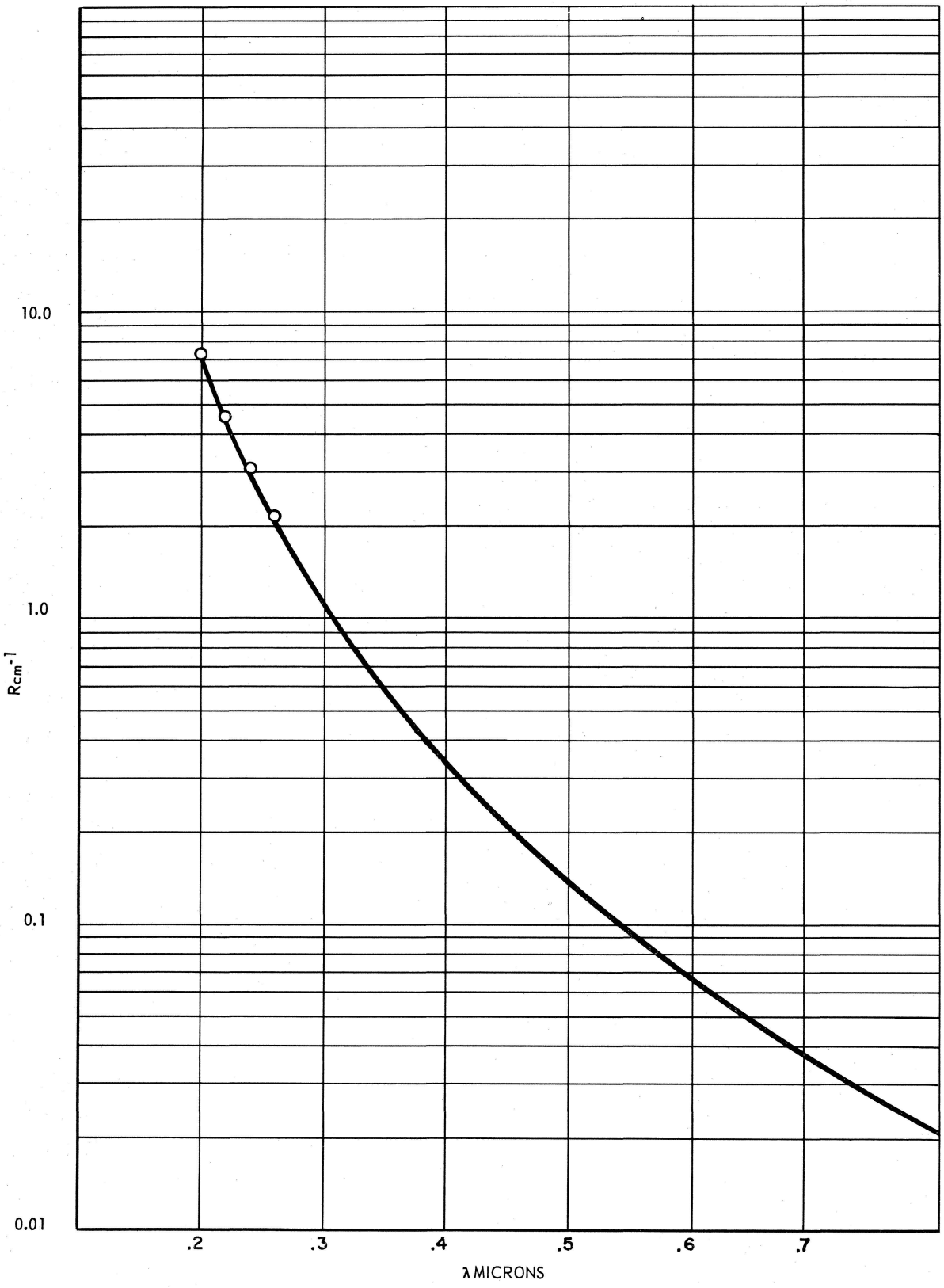

Figure A-3. Atmospheric Scattering

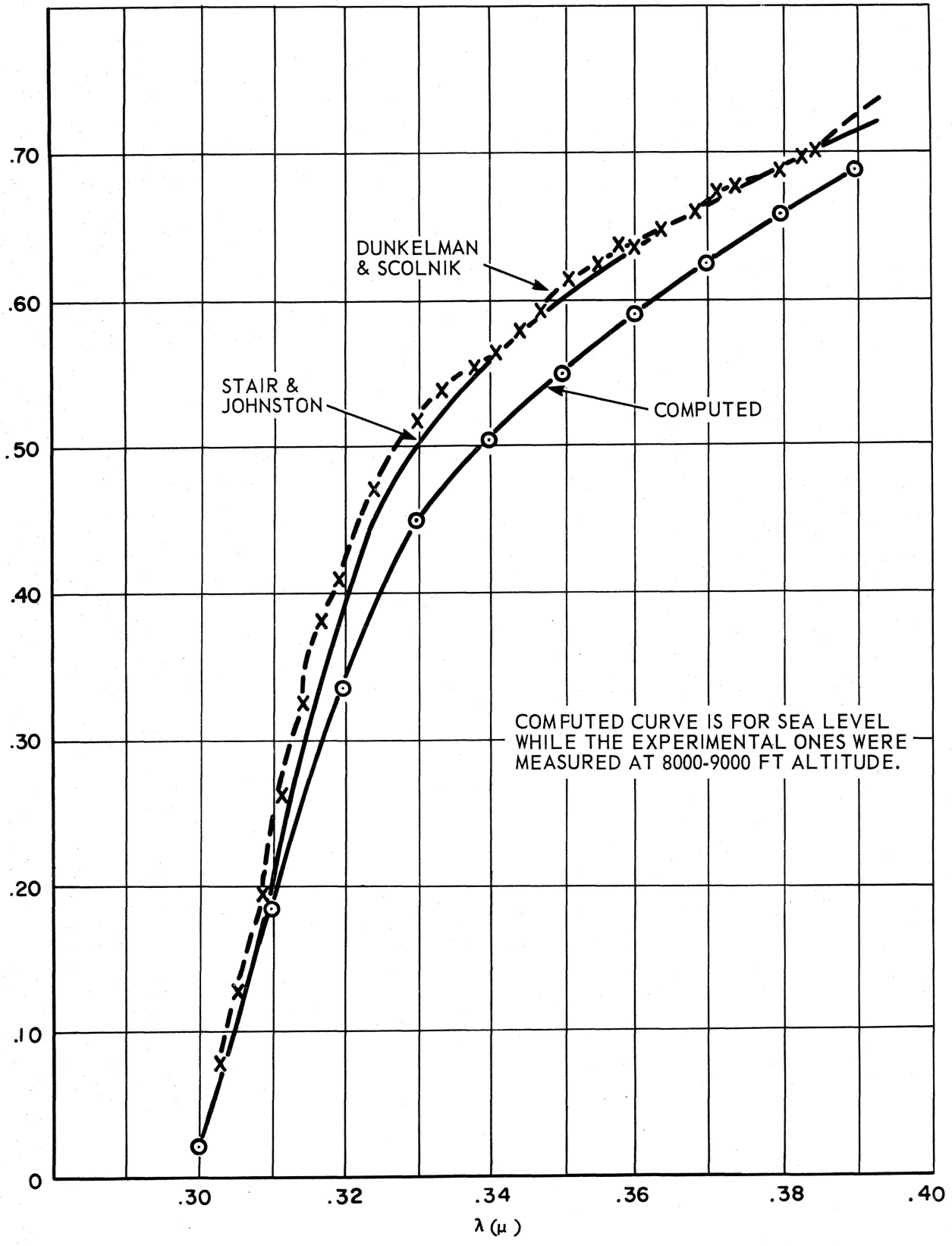

Figure A-4. Vertical Atmospheric Transmission

includes recent rocket measurements as well as ground-based ones. Values adapted from Johnson's data are given in column 2 of table A-2. Computed transmission values are given in the third column and the spectral irradiance expected at sea level in the fourth column. In the final column of table A-2, some of the irradiance values are given in photons incident per cm^2 per second.

This table shows just how sharp the atmospheric cutoff is in the region just below 0.29 micron. The extreme opacity below 0.28 micron is more apparent when it is realized that at 0.275 micron, 1 photon reaches the earth's surface only every 2.2 hours, while at 0.27 micron, 1 photon gets through only every 238 years.

VARIATIONS IN IRRADIANCE

The values of irradiance and of atmospheric transmission given above are for a horizontal surface with the sun at the zenith. If the sun is not at the zenith, the path of sunlight through the atmosphere is greater, producing a lower transmission. If the sun is at an angle z from the zenith, the path length through the atmosphere is m times the zenith path where

$$m = \frac{\text{atmospheric refraction in seconds}}{58.36 \sin z}, \tag{4}$$

and the resultant transmission, T', is

$$T' = T^m, \tag{5}$$

if T is the vertical transmission. The quantity m is known as the optical air mass.

TABLE A-2

SOLAR SPECTRAL IRRADIANCE

Wavelength, λ (μ)	Irradiance, H_o, Outside Atmosphere (μwatts/cm^{2}mμ)	Transmission, T	Irradiance, H, at Sea Level (μw/cm^{2}mμ)	Photons/ cm^{2}sec mμ
0.20	0.30	4.090×10^{-42}	1.227×10^{-42}	
0.21	1.0	2.393×10^{-28}	2.393×10^{-28}	
0.22	3.0	5.256×10^{-23}	1.57×10^{-22}	1.74×10^{-10}
0.23	5.2	1.587×10^{-24}	8.25×10^{-24}	
0.24	5.8	6.537×10^{-30}	3.79×10^{-29}	
0.25	6.4	2.685×10^{-34}	1.72×10^{-33}	
0.26	13.0	1.470×10^{-33}	1.91×10^{-32}	
0.27	25.0	3.904×10^{-24}	9.76×10^{-23}	1.33×10^{-10}
0.275	22.0	4.248×10^{-18}	9.35×10^{-17}	1.29×10^{-4}
0.28	24.0	1.140×10^{-12}	2.74×10^{-11}	3.86×10^{1}
0.285	34.0	4.140×10^{-8}	1.141×10^{-6}	2.02×10^{6}
0.29	52.0	1.481×10^{-5}	7.70×10^{-4}	1.12×10^{9}
0.295	63.0	1.444×10^{-3}	9.10×10^{-2}	1.35×10^{11}
0.30	61.0	2.237×10^{-2}	1.36	2.05×10^{12}
0.305	67.0	9.255×10^{-2}	6.20	
0.31	76.0	0.1830	13.91	
0.315	82.0	0.2780	22.8	
0.32	85.0	0.3355	28.5	
0.325	102.0	0.3942	40.2	
0.33	115.0	0.4493	51.7	
0.34	111.0	0.5041	56.0	
0.35	118.0	0.5494	64.8	
0.36	116.0	0.5891	68.3	
0.37	133.0	0.6237	83.0	
0.38	123.0	0.6557	80.7	
0.39	112.0	0.6852	76.7	

The sunlight is incident on a horizontal surface at the angle z requiring further correction of the irradiance by a factor cos z. Thus, with the sun at a zenith angle z, the irradiance H' on a horizontal surface at sea level is

$$H' = H_o T^m \cos z = HT^{m-1} \cos z \qquad (6)$$

where H_o and H are irradiance on planes perpendicular to the sun's rays above the atmosphere and at sea level, respectively. The zenith distance of the sun can be computed with the equation

$$\cos z = \sin \phi \sin \delta + \cos \phi \cos \delta \cos h, \qquad (7)$$

in which ϕ is the observer's latitude, δ is the sun's declination, and h is the sun's angle hour (the angular distance from the meridian of the observer).

Koller[6] gives the following values for m, computed from equation (4).

Zenith Distance z(°)	0	10	20	30	40	50	60	70	80	85
Cos z	1.000	0.9848	0.9397	0.8660	0.7660	0.6428	0.5000	0.3420	0.1736	0.0872
m	1.00	1.02	1.06	1.15	1.30	1.55	2.00	2.90	5.60	10.40

Using these values of m and cos z, the effect of solar zenith angle on the irradiance can be obtained from equation (6). A few examples are shown in table A-3 in which the values of $T^{m-1} \cos z$ are given in the body of the table for the wavelengths and zenith angles given. It can be seen from the table that the effect of zenith angle is very pronounced at the shorter wavelengths.

TABLE A-3

EFFECT OF ZENITH ANGLE ON THE IRRADIANCE OF A HORIZONTAL PLANE*

λ	T	0°	30°	60°	80°
0.28	1.140×10^{-12}	1	1.40×10^{-2}	5.70×10^{-13}	2.00×10^{-56}
0.285	4.140×10^{-8}	1	6.76×10^{-2}	2.07×10^{-8}	1.90×10^{-35}
0.29	1.481×10^{-5}	1	1.63×10^{-1}	7.41×10^{-6}	1.06×10^{-23}
0.295	1.444×10^{-3}	1	3.25×10^{-1}	7.22×10^{-4}	1.49×10^{-14}
0.30	2.237×10^{-2}	1	4.90×10^{-1}	1.12×10^{-2}	4.45×10^{-9}
0.305	9.255×10^{-2}	1	6.06×10^{-1}	4.63×10^{-2}	3.05×10^{-6}
0.31	0.1830	1	6.71×10^{-1}	9.15×10^{-2}	7.03×10^{-5}
0.35	0.5494	1	7.92×10^{-1}	2.75×10^{-1}	1.10×10^{-2}
0.39	0.6852	1	8.18×10^{-1}	3.43×10^{-1}	3.05×10^{-2}

*The numbers in the body of the table are the ratio ($T^{m-1}\cos z$) of the irradiance at the zenith angle given at the top of the column to that for zero zenith angle.

It should be noted that at most latitudes a zenith angle of 0° is never achieved since the declination, δ, of the sun only varies within the limits $\pm 23.5^{\circ}$ (reference 8, table 169, pages 495 to 496). Thus, from equation (7), a zenith angle of zero can only be obtained at latitudes within the range $\pm 23.5^{\circ}$. Since sin z cannot be zero outside of this latitude belt, equation (4) shows that m cannot reach one at latitudes greater than 23.5°.

SKY LIGHT

In addition to the direct radiation from the sun considered in the preceding discussion, some energy reaches the horizontal surface from all parts of the sky. This sky light is, of course, sunlight scattered from molecules of the atmosphere and from dust particles suspended to it. The ratio of the sky component to the direct solar component on a horizontal surface is shown in figure A-5, which is adapted from figure 8 of Koller.[6] This curve is for the total energy below 0.4 micron and may not be accurate for individual wavelengths. While the sky component for large zenith angles is much larger than the direct solar component, the direct solar component, as shown in table A-3, falls off rapidly with increasing zenith angle. The combined effect is a decrease in total ultraviolet energy with an increase in zenith angle (reference 6, page 118).

The effect of clouds, fog, haze, dust, etc., in the atmosphere is to increase the scattered component but to decrease the direct solar energy. Koller (reference 6, page 130) states that, "The net result, however, is a decrease in the total amount of radiation."

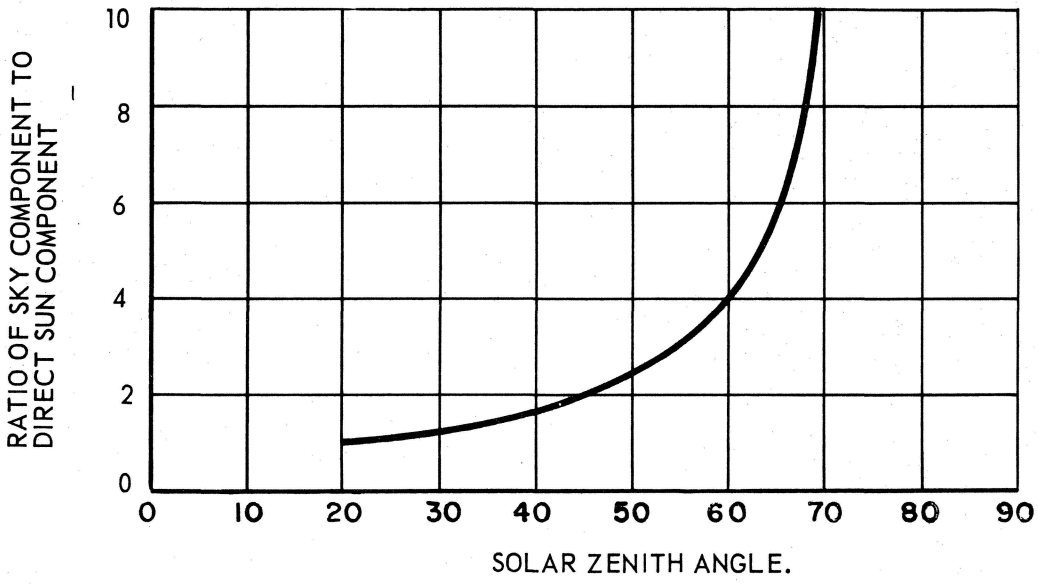

Figure A-5. Ratio of Sky Irradiance on Horizontal Plane to Direct Solar Irradiance as a Function of Solar Zenith Angle

As shown in figure A-5, the sky component for small zenith angles is approximately equal to the direct solar component. Then the maximum ultraviolet irradiance to be expected at ground level is about twice the values of H given in table A-2.

CONCLUSION

Adding the direct sunlight and the sky light gives the combined natural irradiance values for a horizontal surface shown in table A-4 for a perfectly clean atmosphere with the sun at the zenith. The values are the maximum that can be expected, and can only be obtained at latitudes less than 23.5°. At greater latitudes, the sun cannot reach the zenith and lower irradiance values will exist. The maximum values obtainable at the greater latitudes can be computed by multiplying the H_{λ} values in table A-4 by the factor T^{m-1} cos z of equation (6). The maximum value of cos z is computed from equation (7) with δ taken as 23.5° and h as zero. For λ = 0.35 micron, for example, and latitude 45°, T^{m-1} cos z is about 0.89.

TABLE A-4

NATURAL IRRADIANCE AT SEA LEVEL*

λ microns	H $\mu w/cm^2 m\mu$	H Photons/ $sec\ cm^2 m\mu$	H $\mu w/cm^2$	H Photons/sec cm^2
0.20	2.45×10^{-42}	2.47×10^{-30}	1.23×10^{-41}	1.24×10^{-29}
0.21	4.79×10^{-28}	5.06×10^{-16}	4.79×10^{-27}	5.06×10^{-15}
0.22	3.14×10^{-22}	3.48×10^{-10}	3.14×10^{-21}	3.48×10^{-9}
0.23	1.65×10^{-23}	1.91×10^{-11}	3.31×10^{-21}	3.67×10^{-9}
0.24	7.58×10^{-29}	9.16×10^{-17}	3.31×10^{-21}	3.67×10^{-9}
0.25	3.44×10^{-33}	4.33×10^{-21}	3.31×10^{-21}	3.67×10^{-9}
0.26	3.82×10^{-32}	5.00×10^{-20}	3.31×10^{-21}	3.67×10^{-9}
0.27	1.95×10^{-22}	2.65×10^{-10}	4.77×10^{-21}	5.66×10^{-9}
0.275	1.87×10^{-16}	2.59×10^{-4}	9.35×10^{-16}	1.30×10^{-3}
0.28	5.48×10^{-11}	7.73×10^{1}	2.74×10^{-10}	$3.87 \times 10^{+2}$
0.285	2.82×10^{-6}	4.05×10^{6}	1.41×10^{-5}	2.03×10^{7}
0.29	1.54×10^{-3}	2.25×10^{9}	7.71×10^{-3}	1.13×10^{10}
0.295	1.82×10^{-1}	2.70×10^{11}	9.18×10^{-1}	1.36×10^{12}
0.30	2.72	4.11×10^{12}	1.45×10^{1}	2.20×10^{13}
0.305	12.4	1.90×10^{13}	7.65×10^{1}	1.17×10^{14}
0.31	27.8	4.34×10^{13}	2.16×10^{2}	3.34×10^{14}
0.315	45.6	7.23×10^{13}	4.44×10^{2}	6.96×10^{14}
0.32	57.0	9.18×10^{13}	7.29×10^{2}	1.16×10^{15}
0.325	80.4	1.32×10^{14}	1.13×10^{3}	1.82×10^{15}
0.33	103.4	1.72×10^{14}	1.91×10^{3}	3.11×10^{15}
0.34	112.0	1.92×10^{14}	3.03×10^{3}	5.03×10^{15}

TABLE A-4 (continued)

λ microns	H $\mu w/cm^2 m\mu$	Hλ Photons/ sec $cm^2 m\mu$	H $\mu w/cm^2$	H Photons/sec cm^2
0.35	199.6	2.28×10^{14}	4.33×10^{3}	7.31×10^{15}
0.36	136.6	2.48×10^{14}	5.69×10^{3}	9.79×10^{15}
0.37	166.0	3.09×10^{14}	7.35×10^{3}	1.29×10^{16}
0.38	161.4	3.09×10^{14}	9.00×10^{3}	1.60×10^{16}
0.39	153.4	3.01×10^{14}	1.05×10^{4}	1.90×10^{16}

* The spectral irradiance per millimicron band Hλ is given in columns two and three in microwatts per square centimeter and in photons per second per square centimeter. Columns three and four give the total irradiance H due to wavelengths shorter than λ.

REFERENCES

1. A. H. Taylor and G. P. Kerr, "The Distribution of Energy in the Visible Spectrum of Daylight," Journal of the Optical Society of America, 31(1): 3-8, January 1941.

2. R. Stair and R. G. Johnston, "Preliminary Spectroradiometric Measurements of the Solar Constant," Journal of Research of the National Bureau of Standards, 57(4): 205-11, October 1956.

3. L. Dunkelman and R. Scolnik, "Solar Spectral Irradiance," Journal of the Optical Society of America, 49(4): 356-67, April 1959.

4. W. E. Forsythe, Smithsonian Physical Tables, 9th Edition, Smithsonian Institute, Washington, D.C., 1954.

   Table 813, pages 721 and 722, gives the spectral irradiance outside the atmosphere in the range 0.22 to 5.0 microns. Table 815, page 723, gives the spectral irradiance at ground level from 0.295 to 2.14 microns.

5. Optical Society of America, Committee on Colorimetry, The Science of Color, Thomas Y. Crowell Company, New York, 1953. Data for the visual range, 0.38 to 0.78 micron, are given in chapter 8.

6. L. R. Koller, Ultraviolet Radiation, John Wiley and Sons, Inc., New York, 1952. Chapter 4.

7. K. Watanabe, "Ultraviolet Absorption Processes in the Upper Atmosphere," in Advances in Geophysics, Volume 5, 1958, Edited by H. E. Landsberg and J. Van Mieghem, Academic Press, New York, 1958. Table V, page 164.

8. R. J. List, Smithsonian Meteorological Tables, 6th Edition, Smithsonian Institution, Washington, D. C. 1951.

9. E. C. Y. Inn and Yoshio Tanaka, "Absorption Coefficient of Ozone in the Ultraviolet and Visible Regions," Journal of the Optical Society of America, 43(10): 870-73, October 1953.

10. F. S. Johnson, Satellite Environment Handbook, Stanford University Press, Stanford, Calif., 1961. Chapter 4, pages 77-87.

APPENDIX B

SPECTRAL RADIANCE

STANDARDS

APPENDIX B

SPECTRAL RADIANCE STANDARDS

The items used in the calibration with the standard spectral radiance tungsten ribbon lamp were either calibrated by the National Bureau of Standards or directly traceable in Bureau calibrations. The first item used, a current transformer, had a test number 211.03/185915 (which refers to the NBS report number) and a test date of 3 August 1965. The second item, an ac-dc electrodynamometer-type current meter, Weston Model 370, was calibrated at Melpar during July 1965 using a potentiometer and a current shunt. The potentiometer, Guideline Instruments, Ltd. type 9144 (Serial No. 23218), had a test number 211.01/.83081 and a test date of 13 November 1964. The current shunt had a test number 1.3/178643 and a test date of 27 January 1964. The certificate of calibration for the tungsten ribbon radiance standard is reproduced on the following pages.

EPLAB

THE EPPLEY LABORATORY, INC.

SCIENTIFIC INSTRUMENTS

NEWPORT, R.I.

U.S.A.

CERTIFICATE OF CALIBRATION OF A STANDARD OF SPECTRAL RADIANCE

For: Melpar, Inc.,
7700 Arlington Blvd.,
Falls Church, Virginia.

S. O. 13746 **Lamp Serial No.** EPT-1047

1. **Spectral Range of Calibration:** 250 mμ to 2600 mμ.

2. **Method of Calibration**

   See "Instructions for Using the NBS Standards of Spectral Radiance", one copy of which is enclosed. See particularly paragraphs 2 and 3 of the instructions regarding orientation of the standard and portion of the filament viewed.

3. **Standards of Reference**

   The serial numbers of the National Bureau of Standards' reference standards employed are: EU-285 and EU-286.

4. **Results**

   The results are contained in the appended Table.

Tested by: W. A. Simmons

Checked by: J. R. Hickey
Senior Research Physicist

Date: 26 May 1965

TABLE OF RESULTS

Spectral radiance in microwatts per (steradian-nanometer-mm^2 of source)
of lamp No. EPT-1047 operated at 35 amperes

λ (nm ≡ mμ)	Spectral Radiance
250	1.34×10^{-2}
260	2.85×10^{-2}
270	5.33×10^{-2}
280	1.02×10^{-1}
290	1.55×10^{-1}
300	2.44×10^{-1}
320	5.54×10^{-1}
350	1.54
370	2.69
400	5.57
450	1.37 x 10
500	2.68 x 10
550	4.41 x 10
600	6.24 x 10
650	8.27 x 10
700	1.07×10^2
750	1.23×10^2
800	1.37×10^2
900	1.47×10^2
1000	1.52×10^2
1100	1.44×10^2
1200	1.37×10^2
1300	1.26×10^2
1400	1.14×10^2
1500	1.02×10^2
1600	8.99 x 10
1700	7.79 x 10
1800	6.71 x 10
1900	5.87 x 10
2000	5.01 x 10
2100	4.40 x 10
2200	3.82 x 10
2300	3.45 x 10
2400	3.07 x 10
2500	2.75 x 10
2600	2.47 x 10

31426
3/4/66
2 cys